Petrological and experimental constraints on the pre-eruption conditions of holocene dacite from volcan San Pedro (36°S, Chilean Andes)and the importance of sulphur in silicic subduction-related magmas.

Fidel Costa Rodriguez, Bruno Scaillet, Michel Pichavant

JOURNAL OF PETROLOGY | VOLUME 45 | NUMBER 4 | PAGES 855–881 | 2004 | DOI: 10.1093/petrology/egg114

Petrological and Experimental Constraints on the Pre-eruption Conditions of Holocene Dacite from Volcán San Pedro (36°S, Chilean Andes) and the Importance of Sulphur in Silicic Subduction-related Magmas

FIDEL COSTA*, BRUNO SCAILLET AND MICHEL PICHAVANT

INSTITUT DES SCIENCES DE LA TERRE D'ORLÉANS, UMR 6113 CNRS-UO, 1A RUE DE LA FÉROLLERIE, 45071 ORLÉANS, FRANCE

RECEIVED FEBRUARY 4, 2003; ACCEPTED SEPTEMBER 24, 2003

*We present an experimental and petrological study aimed at estimating the pre-eruptive conditions of a Holocene dacitic lava from Volcán San Pedro (36°S, Chilean Andes). Phase-equilibrium experiments were performed at temperatures (*T*) from 800 to 950°C, and mainly at 200 MPa, but also at 55, 150, and 406 MPa. Oxygen fugacity (*fO_2*) ranged from the Ni–NiO buffer (NNO) to 3·5 log units above (NNO + 3·5), and water contents from ~3 to ~6 wt %. We also report several experiments where we added sulphur (0·1–1 wt % S) to the dacite. The main mineral assemblage of the dacite (hornblende + orthopyroxene + plagioclase) is stable at 200 ± 50 MPa, 850 ± 10°C, with 4·5–5·5 wt % H_2O in the melt, and at fO_2 of NNO + 1·2 ± 0·2, in accord with the crystallinity, mineral proportions, and T–fO_2 determination from Fe–Ti oxides of the lava. However, biotite, which is also present in the dacite, is stable at these same T–fO_2 conditions only in experiments with >0·1 wt % S added. This result is in accord with the occurrence of pyrrhotite in the lava, and with the presence of S in glass inclusions and biotite (~300 ppm, and up 170 ppm, respectively). Moreover, the zoning patterns and compositions of plagioclase phenocrysts together with the presence of high-temperature minerals (e.g. clinopyroxene) in the lava suggest that the petrological history of the dacite is more complex than a single near-equilibrium crystallization stage, and could be explained by short-lived (<100 years) temperature fluctuations (~50°C) in the magma reservoir.*

KEY WORDS: *sulphur; dacite; experiments; biotite; Andes*

INTRODUCTION

The pre-eruptive pressure, temperature, volatile content, redox state, and petrology of silicic subduction-related magmas is a highly investigated topic because of the known climatic (e.g. 1982, El Chichón, and 1991, Pinatubo eruptions; Robock, 2000) and potential hazardous effects (e.g. eruptions of Mt. Pelée, 1902, or Mount St. Helens, 1980). Petrological studies that use glass inclusion compositions [e.g. reviews by Johnson *et al.* (1994) and Scaillet & Pichavant (2003)] and geothermobarometers (e.g. Manley & Bacon, 2000) provide a way of partially estimating such parameters, but an alternative and complementary approach is to perform phase equilibrium experiments at various pressures (P), temperatures (T), oxygen fugacities (fO_2), and water fugacities (fH_2O) to reproduce the phase assemblages and compositions of the volcanic products. The experimental approach has been applied to a number of silicic eruptive products, notably: El Chichón (Luhr, 1990), Mount St. Helens (Rutherford *et al.*, 1985; Gardner *et al.*, 1995), Novarupta (Hammer *et al.*, 2002), Mt. Pelée (Martel *et al.*, 1990, 1999; Pichavant *et al.*, 2002), Pinatubo (Rutherford & Devine, 1996; Scaillet & Evans, 1999), Santorini (Cottrell *et al.*, 1999), Soufrière Hills (Barclay *et al.*, 1998), and Unzen (Sato *et al.*, 1999). In most of these studies, the natural phase assemblages were reproduced using a volatile composition consisting mainly of H_2O. The petrological and

*Corresponding author. Present address: Institut für Geologie, Mineralogie, und Geophysik, Ruhr-Universität, Bochum, Bochum 44780, Germany. Telephone: ++49 234 322 4393. Fax: ++49 234 321 4433. E-mail: Fidel.Costa-Rodriguez@ruhr-uni-bochum.de

experimental work carried out on the El Chichón and Pinatubo eruptions, and the abundance of S in glass inclusions in phenocrysts from silicic subduction-related magmas (e.g. Scaillet & Pichavant, 2003), however, show that S can be also an important volatile to take into account for understanding the phase assemblages and composition.

In this paper we combine experimental and petrological data for a Holocene dacitic lava flow from Volcán San Pedro (36°S, Chilean Andes) and we show that its main mineral assemblage (hornblende, plagioclase, and orthopyroxene) and proportions can be experimentally reproduced under a relatively limited set of P, T, fO_2, and $f H_2O$ conditions. However, to explain the full mineral assemblage and textures of the dacite it was also necessary to: (1) perform S-bearing experiments to account for the presence of biotite in the lava at the same pre-eruptive conditions, and (2) to integrate the experimental results with detailed geochemical and petrographical data for the dacite to account for the presence of clinopyroxene and the zoning patterns of plagioclase phenocrysts. The outline of the paper is as follows: after describing the geology and petrography of the San Pedro Holocene zoned eruption we give constraints on the pre-eruptive conditions from the phase assemblage of the dacite alone. Next, we present the experimental results, which include S-free and S-bearing experiments. Finally, we integrate the experimental results with the geochemical and petrographical data for the Holocene magma reservoir, and we discuss whether the pre-eruptive conditions and amount of S inferred for the San Pedro dacite can be applied to other subduction-related dacites.

GEOLOGICAL SETTING AND PRE-ERUPTIVE CONDITIONS ESTIMATED FROM PHASE COMPOSITIONS IN THE DACITIC LAVA

Volcán San Pedro ($\sim 2\,km^3$) is the Holocene volcanic edifice of the Quaternary Tatara–San Pedro volcanic complex (TSPC, 36°S, Chilean Andes; Singer *et al.*, 1997; Dungan *et al.*, 2001; Costa & Singer, 2002). Previous work distinguished between an older phase comprising a main cone-building stage made of basaltic andesitic and dacitic lavas, and a younger phase that post-dated a sector collapse of the eastern flank of the ancestral volcano and included a sequence of lavas that apparently record the downward tapping of a strongly zoned magma chamber (Costa & Singer, 2002). The younger, post-collapse eruptive sequence comprises: (1) $< 0{\cdot}01\,km^3$ of biotite–hornblende dacite; (2) $0{\cdot}2\,km^3$ of biotite–hornblende dacite containing mafic xenoliths (Costa *et al.*, 2002) and quenched mafic inclusions (QMI); (3) $0{\cdot}5\,km^3$ of two-pyroxene dacite with abundant QMI; (4) $0{\cdot}1\,km^3$ of two-pyroxene andesite with rare QMI. The last volcanic activity that rebuilt the summit cone involved basaltic andesites and mafic andesites ($0{\cdot}2\,km^3$). Costa & Singer (2002) proposed that the zoned magma reservoir is the result of incomplete magma mixing between a mafic end-member, represented by the last basaltic andesites, and the first erupted and most silica-rich dacite. We have performed experiments on this silica-rich dacite, which lacks any quenched inclusions, and which we infer to have resided in the upper parts of the San Pedro zoned magma reservoir. Although its bulk-rock composition (66 wt % SiO_2, 2·7 wt % K_2O; Table 1) is similar to older dacites erupted at the TSPC (e.g. Ferguson *et al.*, 1992; Singer *et al.*, 1995; Feeley & Dungan, 1996; Costa & Singer, 2002) or neighbouring volcanoes (e.g. Quizapu; Hildreth & Drake, 1992), its mineral assemblage includes biotite, which appears to be rare in other Holocene dacites erupted in the southern volcanic zone of the Andes (Hildreth & Moorbath, 1988).

Pre-eruptive conditions estimated from the dacite lava phase compositions

The dacite contains ~29 wt % of crystals, mainly plagioclase (~17%) and amphibole (~11%), but also euhedral biotite, clinopyroxene, orthopyroxene, titanomagnetite, ilmenite, apatite, zircon, pyrrhotite, and chalcopyrite, set in a matrix of rhyolitic glass (Table 1). Two or three crystals per thin section of orthopyroxene-mantled olivine (Fo_{82-69}) are also present, and they have been attributed as being derived from basaltic QMI as found in other lavas of the same eruption (Costa & Singer, 2002). Plagioclase phenocrysts are oscillatory zoned and consist of repetitive normal zoning patterns (typically from An_{65} to $\sim An_{50}$), but most rim compositions are An_{40-35} (Singer *et al.*, 1995). There is also a small population of plagioclase xenocrysts (An_{84-82}), which are probably derived from the same mafic inclusions as the olivine xenocrysts (Singer *et al.*, 1995; Costa & Singer, 2002). The proportion of plagioclase xenocrysts is about 10% of the total plagioclase population (Singer *et al.*, 1995), which transferred to wt % of the phases in the lava is about 1·6 wt % and so has little compositional leverage on the bulk-rock composition. Amphibole is magnesiohornblende or tschermakite [classification after Leake *et al.* (1997); hereafter referred to as hornblende *s.l.*], with *mg*-number [= $100MgO/(MgO + FeO^*)$ in moles, where the asterisk indicates total iron as Fe^{2+}] ranging from 62 to 71, and Al_2O_3 contents from 7 to 10 wt % (Table 2). The *mg*-number of biotite ranges from 60 to 66. Both hydrous minerals lack any evidence of destabilization in the form of reaction rims of Fe–Ti oxides or pyroxenes

Table 1: Major and minor element composition of dacitic lava, starting composition, glass inclusions, matrix glass (all normalized to 100% anhydrous), and phase proportions of the dacite

Label:	Dacite bulk-rock	Starting dry glass	Matrix glass	Glass inclusions	Phase proportions	
n:	1	19	10	20	(wt %)	
wt %						
SiO_2	66·0	66·3(0·2)	74·2(0·7)	74·7(1·0)	Pl	16·7
TiO_2	0·51	0·52(0·03)	0·30(0·06)	0·26(0·09)	Hbl	10·5
Al_2O_3	16·32	16·24(0·1)	14·6(0·4)	14·4(0·8)	Ol	<0·5
FeO*	3·75	3·90(0·18)	1·33(0·14)	1·21(0·31)	Cpx	<0·5
MnO	0·08	0·10(0·04)	0·05(0·04)	0·06(0·06)	Opx	<0·5
MgO	1·79	1·71(0·05)	0·18(0·06)	0·15(0·10)	Bt	<0·5
CaO	4·10	4·05(0·08)	1·34(0·13)	1·25(0·36)	Mt	1·5
Na_2O	4·56	4·21(0·10)	4·18(0·11)	4·06(0·56)	Gl	71·2
K_2O	2·72	2·76(0·07)	3·81(0·05)	3·95(0·37)	crystals	28·8
P_2O_5	0·16	0·16(0·06)	n.a.	n.a.	Σr^2	0·6
Total[1]	99·6	98·8(0·3)	98·8(0·4)	96·9(1·6)		
ppm						
S	n.a.	n.a.	<100	294(46)		

FeO*, total iron as Fe^{2+}. *n*, number of analyses. Numbers in parentheses are 2σ deviations of multiple analyses. Dacite bulk-rock composition analysed by XRF (Costa & Singer, 2002). Glass was analysed by electron microprobe (see text for analytical details). Phase proportions were calculated by least-squares mass-balance using the algorithm of Albarède (1995). The error on the calculated plagioclase and hornblende proportions is about 5% relative. Σr^2, squared sum of the residuals. Phase symbols: Pl, plagioclase; Hbl, hornblende; Ol, olivine; Cpx, clinopyroxene; Opx, orthopyroxene; Bt, biotite; Mt, titanomagnetite; Gl, glass. For mass-balance calculations we used the mean composition of the mineral analyses reported in Table 2, plus the composition of the matrix glass, and plagioclase (55 mol % anorthite). The proportions of Ol, Cpx, Opx, and Bt are set to $< 0{\cdot}5$ because the errors from the mass-balance calculations for such a small proportion are around 50% relative. n.a., not analysed.
[1]Original total before normalizing to 100% anhydrous.

(e.g. Rutherford & Hill, 1993; Fougnot *et al.*, 1996). Also present are orthopyroxene ($Wo_{2·7}$, En_{68}, Fs_{29}) and clinopyroxene (Wo_{42}, En_{42}, Fs_{15}; Table 2). The S contents of plagioclase, pyroxenes, and hornblende are below determination (<60 ppm) but biotite has up to 170 ppm, averaging 130 ppm (Table 2). Using the compositions of titanomagnetite and ilmenite that fulfil the equilibrium criteria of Bacon & Hirschmann (1988) we have obtained temperatures of ~840–850°C and fO_2 of ~1·2 log units above the Ni–NiO buffer (NNO) (Huebner & Sato, 1970) using both the Ghiorso & Sack (1991) and the Andersen & Lindsley (1988; QUILF v. 6.42 program of Andersen *et al.*, 1993) Fe–Ti oxide solution models (Table 2).

The interstitial matrix glass is rhyolitic (~74 wt % SiO_2, 3·8 wt % K_2O) with analytical totals close to 100 wt % and a low S content (< 100 ppm), and thus is almost completely degassed (Table 1). In contrast, glass inclusions in orthopyroxene, hornblende, and biotite have low totals, which suggest that at least 3 wt % of water was dissolved in the melt prior to eruption, and also had variable but significant amounts of S (glass inclusions have a mean of ~300 ppm S; Table 1). It should be noted that these volatile contents are probably minimum values because melt inclusions in minerals with good cleavage (e.g. hornblende or biotite) can easily lose their dissolved pre-eruptive volatiles (e.g. Johnson *et al.*, 1994; Gerlach *et al.*, 1996). Despite the difference in volatile contents of the inclusion and matrix glasses, their major element compositions normalized to 100% anhydrous are almost identical (Table 1), which suggests that: (1) to a first approximation, orthopyroxene, hornblende, and biotite crystallized at equilibrium from the same liquid; (2) this liquid was also in equilibrium with the rest of the mineral assemblage, notably plagioclase. These observations are important because they suggest that equilibrium existed between the different phases of the magma, and thus the bulk-rock composition of the lava can be taken as representative of a liquid composition; this is an important assumption for crystallization experiments to determine magma pre-eruptive conditions (see Pichavant *et al.*, in preparation). In summary, the conditions of the dacitic magma prior to eruption estimated from the phase compositions of the lava suggest that it was stored at about 850°C, at an fO_2 of ~NNO + 1·2, and the interstitial melt contained a minimum of 3 wt % H_2O and significant amounts of S (~300 ppm).

Table 2: Representative compositions (wt %) of selected minerals from the San Pedro dacite and T–fO_2 *determination using the compositions of coexisting Fe–Ti oxides*

Mineral:	Clinopyroxene	Orthopyroxene	Hornblende	Biotite
n:	10	12	25	15
SiO_2	51·8(0·5)	52·6(0·7)	43·4(0·9)	36·8(0·4)
TiO_2	0·45(0·10)	0·25(0·4)	2·24(0·33)	4·13(0·14)
Al_2O_3	1·71(0·47)	0·89(0·23)	9·49(0·47)	13·77(0·20)
FeO*	8·88(0·41)	17·99(0·52)	11·80(0·64)	15·51(0·94)
MnO	0·35(0·10)	0·61(0·07)	0·22(0·1)	0·16(0·10)
MgO	14·66(0·50)	24·6(0·4)	13·89(0·52)	13·81(0·68)
CaO	21·4(0·5)	1·37(0·08)	11·07(0·28)	0·01(0·02)
Na_2O	0·31(0·03)	0·02(0·01)	1·92(0·15)	0·92(0·08)
K_2O		0·52(0·08)	8·46(0·13)	
Sum	98·5(0·3)	98·4(0·6)	94·5(0·7)	93·6(0·9)
S (ppm)	b.d.	b.d.	b.d.	130(30)
Wo	42·5(0·9)	2·7(0·2)		
En	42·5(1·3)	68·3(0·9)		
Fs	15·0(0·8)	29·0(0·9)		
mg-no.	74·6(1·4)	70·9(0·9)	67·7(1·8)	61·3(2·5)

Mineral:	Magnetite	Ilmenite		Pyrrhotite	Chalcopyrite
n:	8	6		2	1
SiO_2	0·20(0·32)	0·05(0·04)	Fe	60·3(0·2)	42·0
TiO_2	8·05(1·51)	43·1(0·5)	S	37·6(0·1)	35·2
Al_2O_3	2·25(0·44)	0·3(0·06)	Cu	0·27(0·05)	22·7
FeO*	79·8(2·1)	48·3(0·9)	Sum	98·3(0·3)	99·9
MnO	0·45(0·04)	0·58(0·08)			
MgO	1·50(0·43)	3·04(0·28)			
Total[1]	97·2(0·5)	97·2(1·1)			
				G&S	A&L
Fe_2O_3c	49·7(3·3)	17·2(1·9)	T°C	850	840
FeO*c*	35·1(1·0)	32·8(0·8)	log fO_2	−11·7	−11·8
*X*Ulv	0·24(0·05)		ΔNNO	1·1	1·2
*X*Ilm		0·82(0·02)			

FeO*, total iron as Fe^{2+}; *mg*-number = 100MgO/(MgO + FeO*) in moles. Pyroxene end-members: Wo, wollastonite; En, enstatite; Fs, ferrosilite; calculated according to Deer *et al*. (1992). *n*, number of analyses. Numbers in parentheses are the 2σ of multiple analyses. *X*Ulv, ulvöspinel mol fraction; *X*Ilm, ilmenite mol fraction. G&S indicates Ghiorso & Sack (1991) and A&L indicates Andersen & Lindsley (1988) calibrations of Fe–Ti oxide solution models. ΔNNO, oxygen fugacity above the Ni–NiO buffer of Huebner & Sato (1970). b.d., below determination (~60 ppm). The letter '*c*' denotes calculated.
[1]Total after recalculating the proportions of Fe^{3+} and Fe^{2+} with the structural formula (Stormer, 1983).

EXPERIMENTAL AND ANALYTICAL TECHNIQUES

Selection of experimental conditions

Crystallization experiments were mainly performed at 200 MPa, in the temperature range of 800–950°C, at intervals of 25°C (Table 3). Melt water contents ranged from ~3 to 6 wt %, and fO_2 was varied from NNO to NNO + 3·5. At the pre-eruptive temperature determined with the Fe–Ti oxides of the lava (850°C) we carried out three experiments at different fO_2 (NNO, NNO + 1·4, and NNO + 3) to check for the effect of fO_2 on mineral stabilities. In addition, we also performed S-bearing experiments from 800 to 900°C, at 200 MPa, with fO_2 varied from NNO + 1·4 to NNO + 3·5. Two experiments were performed at lower pressures (55 and 150 MPa), and 850°C, and one at 406 MPa.

Table 3: Experimental conditions, run products, and phase proportions

Charge	Starting material	ΔNNO[1]	XH_2O_{in}[2]	H_2O in melt (wt %)[3]	Phase proportions (wt %)[4]	Σr^2
P = *206 MPa*, T = *850 °C, run duration = 163 h, IHPV*						
1	dry glass	0·3	1·00	6·0	Gl(75·9), Hbl(12·2), Pl(11·0), Mt(0·8)	1·5
2	dry glass	0·2	0·89	5·4	Gl(66·5), Hbl(12·0), Opx(<0·5), Pl(20·0), Mt(1·2)	0·7
4	dry glass	0·0	0·68	4·2	Gl(57·9), Hbl(9·7), Opx(1·9), Pl(29·1), Mt(1·4)	0·2
5	dry glass	−0·2	0·55	3·6	Gl(53·1), Opx(8·9), Pl(37·2), Mt(0·8)	1·1
6	dry glass	−0·3	0·5		Gl, Opx, Pl, Mt	
7	dry glass	−0·7	0·3		Gl, Opx, Pl, Mt, Qtz	
P = *206 MPa*, T = *900 °C, run duration = 165 h, IHPV*						
8	dry glass	1·3[5]	1·00	6·0	Gl(91·8), Hbl(5·0), Pl(1·8), Mt(1·5)	0·8
9	dry glass	1·2[5]	0·91	5·4	Gl(84·9), Hbl(6·3), Pl(7·3), Mt(1·6)	0·7
10	dry glass	1·1[5]	0·82	4·9	Gl(74·8), Hbl(6·6), Opx(<0·5), Pl(16·4), Mt(2·0)	0·1
11	dry glass	1·0[5]	0·70	4·1	Gl(66·4), Opx(2·3), Cpx(2·4), Pl(25·6), Mt(2·3)	0·5
12	dry glass	0·9[5]	0·60		Gl, Opx, Cpx, Pl, Mt	
13	dry glass	0·8[5]	0·5		Gl, Opx, Cpx, Pl, Mt	
14	dry glass	0·7[5]	0·4		Gl, Opx, Cpx, Pl, Mt	
P = *207 MPa*, T = *950 °C, run duration = 164 h, IHPV*						
17	dry glass	2–3·5[6]	0·91	5·2	Gl(96·7), Cpx(0·8), Mt(2·5)	0·4
18	dry glass	2–3·5[6]	0·81	4·5	Gl(89·5), Cpx(2·2), Pl(6·0), Mt(2·4)	0·2
19	dry glass	2–3·5[6]	0·71	4·0	Gl(76·4), Cpx(1·0), Opx(1·8), Pl(17·9), Mt(2·9)	0·1
20	dry glass	2–3·5[6]	0·61	3·5	Gl(67·9), Cpx(1·2), Cpx(2·5), Pl(25·4), Mt(3·0)	0·1
21	dry glass	2–3·5[6]	0·5	3·2	Gl(53·3), Cpx(1·8), Opx(2·8), Pl(39·0), Mt(3·1)	0·1
22	dry glass	2–3·5[6]	0·4	2·5	Gl(49·6), Cpx(1·3), Opx(3·1), Pl(42·8), Mt(3·2)	0·1
P = *195 MPa*, T = *850 °C, run duration = 168 h, IHPV*						
24	dry glass	2·5–3·5[7]	1·00	5·8	Gl(72·5), Hbl(8·5), Pl(16·2), Mt(2·9)	1·6
26	dry glass	2·5–3·5[7]	0·80	4·7	Gl(61·8), Hbl(6·9), Pl(28·2), Mt(3·1)	0·1
27	dry glass	2·5–3·5[7]	0·69	4·2	Gl(57·1), Opx(3·9), Pl(35·3), Mt(3·7)	0·4
28	dry glass	2·5–3·5[7]	0·61	3·8	Gl(54·1), Opx(4·1), Pl(38·2), Mt(3·6)	0·3
P = *200 MPa*, T = *925 °C, run duration = 144 h, IHPV*						
33	dry glass	2·8–3·5[6]	0·85	4·9	Gl(85·9), Cpx(< 0·5), Hbl(3·4), Pl(8·2), Mt(2·9)	0·1
34	dry glass	2·8–3·5[6]	0·78	4·5	Gl(78·8), Cpx(< 0·5), Hbl(4·2), Pl(14·3), Mt(3·1)	0·2
35	dry glass	2·8–3·5[6]	0·65	3·8	Gl(68·4), Cpx(2·1), Opx(1·7), Pl(24·5), Mt(3·3)	0·2
36	dry glass	2·8–3·5[6]	0·5	3·3	Gl(61·3), Cpx(2·6), Opx(2·1), Pl(30·5), Mt(3·5)	0·2
37	dry glass	2·8–3·5[6]	0·4	2·8	Gl(57·0), Cpx(2·9), Opx(2·0), Pl(34·8), Mt(3·4)	0·1
P = *206 MPa*, T = *875 °C, run duration = 163 h, IHPV*						
40	dry glass	1·2	1·00	6·0	Gl(82·5), Hbl(9·8), Pl(6·3), Mt(1·4)	1·7
41	dry glass	1·2	0·94	5·6	Gl(78·0), Hbl(10·2), Pl(9·8), Mt(2·0)	1·8
46cr	crushed rock	1·2	1·00	6·0	Gl(84·1), Hbl(7·3), Pl(7·5), Mt(1·2)	0·9
P = *206 MPa*, T = *900 °C, run duration = 120 h, IHPV*						
47	dry glass	1·3	1·00	6·0	Gl(86·8), Hbl(10·2), Pl(1·7), Mt(1·3)	1·8
51s	dry glass + 1 wt % S	1·3	1·00	6·0	Gl(85·3), Hbl(11·6), Pl(1·9), Po(0·6)	2·0

Table 3: Continued

Charge	Starting material	ΔNNO[1]	XH_2O_{in}[2]	H_2O in melt (wt %)[3]	Phase proportions (wt %)[4]	Σr^2
P = *405 MPa*, T = *850°C, run duration = 164 h, IHPV*						
67	dry glass	1·9	1·00		Gl, Hbl, Mt	
69	dry glass	1·8	0·91		Gl, Hbl, Mt	
71	dry glass	1·6	0·70		Gl, Hbl, Pl, Mt	
P = *200 MPa*, T = *875°C, run duration = 264 h, IHPV*						
81s	dry glass + 1 wt % S	3[8]	1·00	6·0	Gl(93·2), Bt(1·4), Pl(< 0·5), Mt(3·5), Anhy(1·9)	0·3
86	dry glass	3[8]	1·00	6·0	Gl(84·2), Hbl(5·9), Pl(7·3), Mt(2·6)	0·5
87s	dry glass + 0·5 wt % S	3[8]	1·00	6·0	Gl(87·8), Bt(1·9), Pl(5·4), Mt(3·8), Anhy(1·0)	0·3
88s	dry glass + 0·1 wt % S	3[8]	1·00	6·0	Gl(85·4), Hbl(5·3), Pl(6·0), Mt(2·9), Anhy(< 0·5)	0·2
P = *200 MPa*, T = *850°C, run duration = 158 h, IHPV*						
89s	dry glass + 1 wt % S	1·4	1·00	5·9	Gl(76·1), Hbl(9·0), Pl(12·3), Bt(< 0·5), Mt(1·3), Anhy(< 0·5), Po(0·7)	1·2
94	dry glass	1·4	1·00	5·9	Gl(75·7), Hbl(10·3), Pl(12·2), Mt(1·8)	1·1
95s	dry glass + 0·5 wt % S	1·4	1·00	5·9	Gl(72·9), Hbl(10·2), Pl(14·3), Bt(< 0·5), Mt(1·5), Anhy(< 0·5), Po(< 0·5)	1·1
96s	dry glass + 0·1 wt % S	1·4	1·00	5·9	Gl(73·4), Hbl(11·5), Pl(13·3), Mt(0·4), Po(1·4)	1·2
P = *203 MPa*, T = *875°C, run duration = 240 h, IHPV*						
97	dry glass	1·2[9]	1·00	6·0	Gl(86·3), Hbl(7·4), Pl(5·6), Mt(0·8)	0·5
98s	dry glass + 1 wt % S	1·2[9]	1·00	6·0	Gl(82·7), Hbl(8·7), Pl(8·6), Po(1·6)	0·5
P = *200 MPa*, T = *800°C, run duration = 420 h, CSPV*						
108	dry glass	3–4[7]	1·00	6·1	Gl(61·4), Hbl(8·4), Bt(0·6), Pl(26·6), Mt(3·0)	0·1
109s	dry glass + 1 wt % S	3–4[7]	1·00	6·1	Gl(68·5), Bt(5·2), Pl(20·8), Mt(3·7), Anhy(1·8)	0·2
P = *200 MPa*, T = *825°C, run duration = 168 h, IHPV*						
133	dry glass	1·4–2·5[10]	1·00	5·9	Gl(66·9), Hbl(10·6), Pl(20·8), Mt(1·8)	3·0
137s	dry glass + 1 wt % S	1·4–2·5[10]	1·00	5·9	Gl(68·5), Hbl(9·0), Pl(20·6), Bt(< 0·5), Mt(1·9), Anhy(< 0·5), Po(< 0·5)	1·6
P = *208 MPa*, T = *850°C, run duration = 158 h, IHPV*						
141cr	crushed rock	2·5–3·5[7]	1·00	6·0	Gl(77·1), Hbl(7·7), Pl(12·6), Mt(2·7)	0·5
142	dry glass	2·5–3·5[7]	1·00	6·0	Gl(73·6), Hbl(7·7), Pl(15·9), Mt(2·7)	1·6
143	dry glass	2·5–3·5[7]	0·80	4·7	Gl(62·8), Hbl(6·7), Pl(27·3), Mt(3·2)	0·8
144s	dry glass + 1 wt % S	2·5–3·5[7]	1·00	6·0	Gl(84·8), Bt(4·2), Pl(4·8), Mt(4·2), Anhy(2·0)	1·5
146s	dry glass + 1 wt % S (as H_2SO_4)	2·5–3·5[7]	1·00	6·0	Gl(83·8), Bt(4·1), Pl(6·8), Mt(3·9), Anhy(1·8)	0·8
148s	dry glass + 1 wt % S (as Anhy powder)	2·5–3·5[7]	1·00	6·0	Gl(81·1), Bt(4·5), Pl(8·8), Mt(4·0), Anhy(1·6)	1·1
P = *150 MPa*, T = *850°C, run duration = 158 h, IHPV*						
184	dry glass	0·9	1·00	4·9	Gl(63·0), Hbl(11·4), Opx(< 0·5), Pl(24·3), Mt(1·3)	0·3
186	dry glass	0·7	0·75	3·9	Gl(53·8), Opx(7·4), Pl(36·7), Mt(2·0)	1·9
P = *54 MPa*, T = *850°C, run duration = 230 h, IHPV*						
190	dry glass	2·5–3·5[7]	1·00		Gl, Opx, Pl, Mt	

Charge	Starting material	ΔNNO[1]	XH_2O_{in}[2]	H_2O in melt (wt %)[3]	Phase proportions (wt %)[4]	Σr^2
P = *211 MPa*, T = *875°C, run duration = 146 h, IHPV*						
201	dry glass	2·5–3·5[7]	0·76	4·6	Gl(65·9), Hbl(6·4), Pl(24·8), Mt(2·9)	0·3
202	dry glass	2·5–3·5[7]	0·5		Gl, Opx, Pl, Mt	

[1]NNO = log fO_2 (experiment) − log fO_2 at Ni–NiO buffer of Huebner & Sato (1970). For water-undersaturated runs, the maximum fO_2 was calculated as log fO_2 = log fO_2 (at water saturation) + 2 log XH_2O_{in}.
[2]XH_2O_{in} = $H_2O/(H_2O + CO_2)$ loaded in the capsule in mols.
[3]H_2O calculated by mass-balance and using the H_2O–CO_2 solubility model for rhyolitic composition of Tamic *et al.* (2001). For the almost water-saturated, S-bearing runs, the presence of sulphur in the fluid phase was not taken into account for calculating the water in the melt but its proportion is almost negligible (see text for more details).
[4]Phase proportions calculated by least-squares mass-balance using the algorithm of Albarède (1995). Relative errors are <3% for a phase >50 wt %, <5% for a phase 20–50 wt %, <10% for a phase 2–20 wt %, and >10% for a phase <2 wt %.
[5]fO_2 estimated to be the same as for experiment 47 because hornblende has the same *mg*-number (e.g. Scaillet & Evans, 1999).
[6]Estimated using NiPd sensor (Pownceby & O'Neill, 1994).
[7]Intrinsic oxygen fugacity of the pressure vessel.
[8]fO_2 estimated to be this value because only anhydrite was found in the S-bearing experiments.
[9]fO_2 estimated to be the same as for experiment 41 because hornblende has the same *mg*-number.
[10]fO_2 estimated to be this value because anhydrite and pyrrhotite coexist in the S-bearing experiment (e.g. Carroll & Rutherford, 1987; Scaillet & Evans, 1999).
Σr^2, squared sum of the residuals. The letter 's' after the charge number indicates that S was added to the starting material, whereas the letters 'cr' indicate that the starting material is the crushed rock. IHPV, internally heated pressure vessel; CSPV, cold seal pressure vessel. Phase symbols are the same as in Table 1, plus: Qtz, quartz; Po, pyrrhotite; Anhy, anhydrite.

Starting products and preparation of the charges

The dry glass used as starting material for most experiments was prepared by fusing twice (grinding between fusions in an agate mortar) the dacite powder in Pt containers at 1400°C and atmospheric pressure for 3–4 h. The starting glass was analysed by electron microprobe and was found to be homogeneous and of the same composition as the bulk-rock determined by X-ray fluorescence (XRF), except for somewhat lower Na_2O contents (Table 1). Two experiments were performed using the dacite lava crushed in an agate mortar.

The dry glass powder was loaded in Au capsules of 15 mm length, 2·5 mm internal diameter, and 0·2 mm wall thickness. All experiments were fluid-saturated and deionized H_2O, CO_2 (as silver oxalate), and the dry glass powder (~0·03 g) were added as described by Scaillet *et al.* (1995), with fluid/silicate weight values of 0·11–0·13, except for the experiment at 406 MPa, where the fluid/silicate weight values were 0·13–0·15. Most of the experiments with added S were prepared by mixing elemental sulphur and dry glass powder at a concentration of 1 wt % S, from which lower concentrations of S in the starting material were obtained by addition of the S-free dry glass. In one experiment we added S in three forms to check if we obtained the same results: (1) S added as elemental S; (2) S added as anhydrite; (3) S added as H_2SO_4. For the experimental conditions (850°C, NNO + 3) and the amount of S added (1 wt %), the phase proportions and compositions of the three runs are almost the same. It should be noted that because S partitions into the fluid and into S-bearing minerals, the wt % S added in the capsules is significantly higher than the amount of S present in the glass.

The arc-welded capsules were left at ~100°C for 6–12 h in an oven to improve homogenization of the water distribution within the capsule before starting the experiments. For all the runs reported in the tables, the weight of the loaded capsule prior to welding, after welding, after 6–12 h at ~100°C, and after the experiment agreed to within 0·0003 g, which is about the precision of the analytical balance, and ensures that no fluid escaped during the experiments. Uncertainties in the fluid composition loaded into the capsules, which we call XH_2Oin [= initial $H_2O/(H_2O + CO_2)$ in moles], are ~2% relative for $0·7 < XH_2Oin < 1$, ~5% for $0·5 < XH_2Oin < 0·7$, and up to 30% for $XH_2Oin < 0·5$. It should be noted that the reported XH_2Oin values for the experiments with added sulphur do not take into account the dilution of H_2O by the presence of S. None the less, the low amounts of S added (0·1–1 wt % of the dry glass) do not have a very significant effect on XH_2Oin. For example, if we suppose that all S added goes into the fluid phase in an experiment in which we added 1 wt % S, then the reported XH_2Oin values are lower by about 5% relative (i.e. instead of $XH_2Oin = 1$, we have $XH_2Oin = 0·95$). If we make a more realistic estimate using the mass-balance constraints for the amount of S that will be locked into ~1 wt % of sulphur-bearing minerals (anhydrite and/or pyrrhotite), we find that at most 50 wt % of the initial S

loaded into the capsule will be in the fluid phase. This lowers the XH_2O_{in} values by about 2% relative, which is about the precision of the analytical balance that we have used.

Experimental equipment

The experimental equipment used in this study is the same as that used and described by Scaillet & Evans (1999), thus only basic information is given here. All experiments were performed at the ISTO-CNRS-Orléans using internally heated pressure vessels (IHPV) working vertically, and in cold-seal pressure vessels (CSPV) working horizontally. The pressure medium was Ar or a mixture of Ar + H_2 obtained by sequential loading at room temperature. Total pressure was continuously monitored by transducers calibrated against a Heise Bourdon tube gauge with an uncertainty of ~2 MPa. In the IHPV, temperatures were recorded by two or three sheathed, type-K thermocouples, whereas in the CSPV, external unsheathed type-K thermocouples (calibrated against NaCl at 0·1 MPa) were used. Temperature gradients in the hotspot zones were <10°C, with a temperature uncertainty of ~5°C (Scaillet *et al.*, 1992; Schmidt *et al.*, 1995). Experiments were brought from room temperature directly to run temperature in about 30–60 min. Typically, 3–7 capsules with different fluid composition were run in the same experiment. Experiments performed with a Shaw-type membrane (in IHPV) for the control of H_2 fugacity (Scaillet *et al.*, 1992) were quenched isobarically and terminated by switching off the power supply, which resulted in cooling rates of ~100°C/min. A fast-quench device (Roux & Lefèvre, 1992) was used in other experiments run in IHPV, and the sample holder fell instantaneously into the coldest part of the vessel (~50°C). Experiments performed with CSPV were terminated by removing the vessel from the furnace and tilting it, so that the capsules fell instantaneously into the coldest part of the vessel (~25°C).

Control and calculation of fH_2, fH_2O, and fO_2

The redox states of the experimental charges without the fast-quench device were controlled by the fH_2 of the fluid pressure medium. The fH_2 was continuously read with a Shaw membrane connected to transducers, with an uncertainty of 0·02 MPa [for more details see Scaillet & Evans (1999)]. The fO_2 was calculated from the reaction $H_2O = H_2 + \frac{1}{2}O_2$, using the fH_2O for pure water from Burnham *et al.* (1969) and the dissociation constant of H_2O from Robie *et al.* (1979), with an overall uncertainty on fO_2 of ~0·2 log units. For runs with added CO_2, the maximum fO_2 was calculated assuming ideal mixing in the fluid phase and constant fH_2, and using the relation $\log fO_2 = \log fO_2$ (at $XH_2O = 1$) + 2 log XH_2O_{in}. This estimation is a maximum because the final XH_2O in the fluid is always lower than the initial XH_2O_{in} loaded in the capsule, as a result of preferential dissolution of H_2O in the melt relative to CO_2. In experiments where the Shaw membrane was not used, the fO_2 was calculated using a solid sensor of hand-pressed Ni–Pd–NiO pellets and the formulation of Pownceby & O'Neill (1994). In experiments where the Ni–Pd–NiO pellets did not work (usually because a small amount of S was present), we have given a range of fO_2 values, which were estimated by: (1) the intrinsic fO_2 of the pressure vessel; (2) comparison of mineral compositions between charges at the same T–P (typically the *mg*-number of hornblende; Scaillet & Evans, 1999); (3) the stability of anhydrite and pyrrhotite in S-bearing runs (Carroll & Rutherford, 1987; Scaillet & Evans, 1999).

The water contents of the glasses were calculated in two ways: (1) using the by-difference method, in which the difference between the electron microprobe totals and 100% was calibrated using four standards of rhyolitic composition containing ~0–6·4 wt % water determined by Karl Fischer titration (Scaillet & Evans, 1999); (2) by iteratively calculating the fluid composition by mass-balance and the empirical solubility model for mixed H_2O–CO_2 fluids of Tamic *et al.* (2001). In general, the calculated water contents with the Tamic *et al.* (2001) model are 1–3 wt % (absolute) lower that those estimated with the by-difference method, which is probably due to incipient exsolution of vapor producing micrometre-sized H_2O bubbles that decrease the microprobe total (e.g. Scaillet & Evans, 1999). For constructing the phase diagrams and data description and discussion we use the calculated values from the model of Tamic *et al.* (2001), which have ~5% relative error.

Analytical techniques

Run products were examined with a reflected and transmitted light microscope and by scanning electron microscopy (SEM), and were analysed with an electron microprobe. Analytical conditions for the electron microprobe (Cameca SX-50 instrument of the CNRS-BRGM at Orléans) were: accelerating voltage of 15 kV, sample current of 6 nA for glasses and 12 nA for minerals, a beam diameter of ~10 μm for glasses and <4 μm for minerals, with counting times of 10 s on peak for all elements in the glass (Na and K were always analysed first) and 20 s for minerals, and a ZAF correction. The Na contents for glasses with about ~6 wt % H_2O were corrected for Na loss (e.g. Luhr, 1990), which at these analytical conditions was at most ~15% relative, and negligible for glasses with <5 wt % H_2O. The corresponding increase of Si concentration was <1% for glasses with ~6 wt % H_2O and has not been corrected for. Sulphur analyses of the glasses were performed by calibration with three rhyolitic glasses with S contents varying from 750 to 1900 ppm with the S peak position

determined for pyrrhotite. We used an accelerating voltage of 15 kV, sample current of 50 nA, and a beam diameter < 4 μm. The sulphur counts were measured in three PET spectrometers simultaneously for 60 s in the peak and 60 s in background. Counting statistics show that under these conditions the level of detection (three times the square root of the background counts) is ~50 ppm, whereas the determination is ~100 ppm. The analyses of silicate minerals from the lava for which S was determined were obtained with a Cameca SX-50 instrument (Ruhr-Universität, Bochum) using 15 kV, 100 nA, and a beam size of 25 μm × 25 μm. Three minutes were counted on the S peak and also on the background; under these conditions the level of detection is ~60 ppm.

Attainment of equilibrium

The experimental technique that we have employed consists of performing long runs (typically a week) using homogeneous glasses as starting materials, both of which should favour attainment of equilibrium conditions compared with melting experiments. Scanning electron micrographs of the charges show that minerals are unzoned (Fig. 1), and intercrystalline compositional variation is typically small as shown by the small standard deviations of the electron microprobe analyses of the glass and minerals. In some rare charges, hornblende crystals contain small clinopyroxene cores, and plagioclase shows a relatively large spread in composition (but always <5 mol % An). We interpret this as due to some heterogeneity in the distribution of the silver oxalate and water at the beginning of the experiments. This problem was largely avoided by leaving the welded capsules at ~100°C for 6–12 h in an oven prior to experiments. Another observation that suggests that equilibrium was attained is that phase proportions and compositions change in a coherent way with temperature or water contents (see below). The charges from two experiments using the crushed dacite as starting material show prominent mineral zoning (as observed by SEM) and large variations in mineral compositions (see also Scaillet & Evans, 1999), although the glass composition is fairly homogeneous and mineral proportions are similar to those in the charges using dry glass as starting material. The results from these melting experiments have not been plotted in the figures.

EXPERIMENTAL RESULTS

General textural and mineralogical observations on the experimental charges

Crystals are typically euhedral (Fig. 1) and can be homogeneously distributed or not, in which case glass tends to form pools. Despite this textural difference no significant compositional difference was found in glass or minerals from different locations within the same charge. Crystals

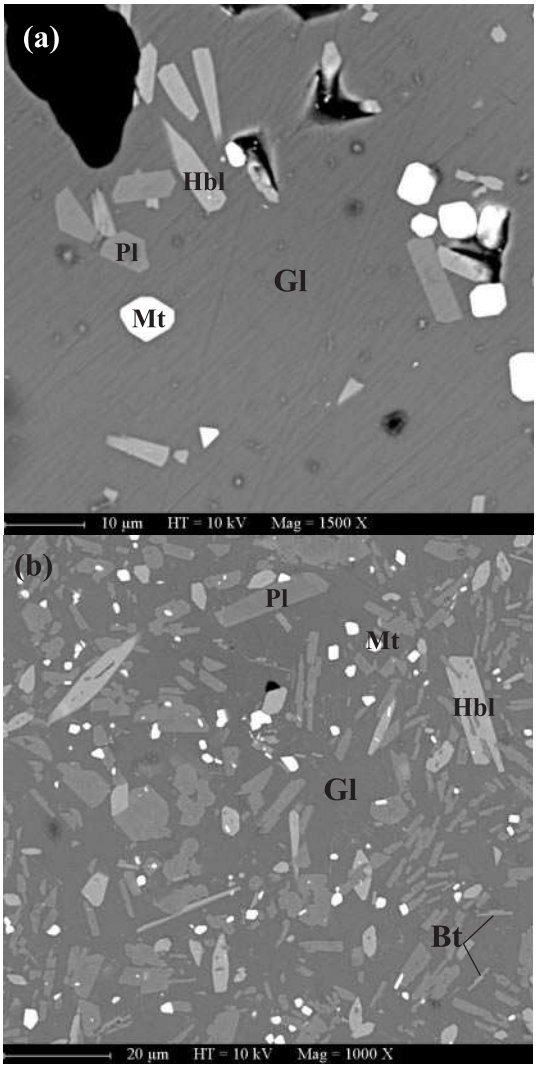

Fig. 1. Scanning electron micrographs of selected experimental charges. (a) Charge 8 (900°C, 200 MPa, 6 wt % H_2O) contains ~92 wt % glass (Gl) and crystals of plagioclase (Pl), hornblende (Hbl), and titanomagnetite (Mt). It should be noted that crystals are not zoned and are euhedral. (b) Charge 108 (800°C, 200 MPa, 6 wt % H_2O) contains ~60 wt % glass, plus hornblende, plagioclase, titanomagnetite, and small biotite crystals (Bt).

are in general small (commonly < 20 μm; Fig. 1), so during electron microprobe analyses in some cases it was difficult or impossible to avoid contamination with the glass or other minerals. Phase compositions are reported as means, and represent the best electron microprobe analyses that fulfilled structural formula constraints; however, the significance of minor element variation with intensive variables in the experimental crystals should be treated with caution. In runs where it was not possible to analyse one of the minerals, we have used the composition of the same mineral from a different charge run at the same T and P, but with slightly different fluid composition for mass-balance purposes (Table 3). For

one charge (11) at 900°C we used the composition of the clinopyroxene at 925°C; for two charges at 850°C (27 and 28) we used the orthopyroxene composition of charge 19, run at 925°C but at a very similar fO_2; and for charge 51 s we used the plagioclase composition of charge 47. In addition, we have recalculated the composition of a biotite (108) and two plagioclases (26 and 28) by subtracting the glass composition until a reasonable stoichiometric analysis was obtained. Quartz has been recognized only in one charge. Although apatite and ilmenite were detected by SEM in some charges, they have not been quantitatively analysed and no efforts have been made to define their stability limits. Charges 40, 41, and 46cr (run at 875°C), and charges 47 and 51 s (run at 900°C) display textural evidence of quench phases: thus, they have slightly higher crystal contents and more evolved glass compositions than charges run at the same conditions that were perfectly quenched. The experiment at 406 MPa was not quenched fast enough so glasses have not been analysed and phase proportions have not been calculated. In charges with very low water contents or run at low total pressures, phases could not be quantitatively analysed because of their small size.

Phase relations, proportions, and composition of S-free charges

In S-free experiments performed at ~200 MPa, titanomagnetite and clinopyroxene are the near-liquidus minerals at 950°C and ~5 wt % H_2O (Fig. 2). Titanomagnetite remains stable over the entire investigated temperature and water content range, whereas clinopyroxene tends to be stable in water-poor experiments and at high temperature; it has not been identified at or below 875°C. Plagioclase is stable throughout the investigated T–fO_2–fH_2O range except in one charge with ~5 wt % H_2O at 950°C. Hornblende is stable at 925°C and at lower temperatures in the water-rich part of the diagram (4–6 wt % H_2O). Orthopyroxene occurs at all investigated temperatures, but tends to be stable in the water-poor part of the diagram (e.g. <5 wt % H_2O); its stability field depends on fO_2, being more stable at more reduced conditions (Fig. 2). Quartz has been identified only in one charge at 850°C and low water content (<3·6 wt %). Biotite was found only at 800°C and NNO + 3. At these same T–fO_2 conditions, biotite was also not found when we used the crushed dacite as starting material (charge 141cr), and thus the absence of biotite does not depend on the experimental procedure (e.g. melting or crystallization). At 150 MPa and 850°C the mineral assemblage is the same as that at 200 MPa (but orthopyroxene is found at water-saturated conditions). At 55 MPa, 850°C, and water-saturated conditions, orthopyroxene replaces hornblende, and clinopyroxene has not been identified. The experiment carried out at 405 MPa and 850°C shows that at water-saturated conditions (~9 wt % H_2O in the melt) hornblende and titanomagnetite are the only stable minerals, and lower water contents are necessary to stabilize plagioclase (~6 wt % H_2O).

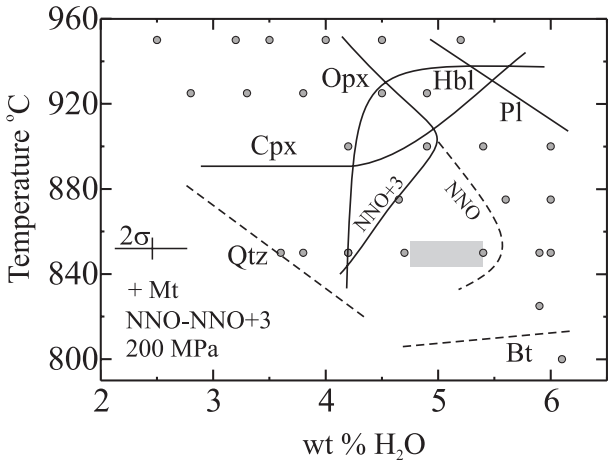

Fig. 2. Phase relations of the San Pedro dacite at ~200 MPa without added sulphur. The wt % H_2O refers to water in the glass. Curves labelled with minerals lying in their stability field. Dashed lines indicate that the stability field of the mineral is not very well constrained. Grey box shows the fO_2 and temperature estimated from the Fe–Ti oxides of the dacitic lava. Mineral symbols as in Fig. 1, plus: Cpx, clinopyroxene; Opx, orthopyroxene; Qtz, quartz. The stability of orthopyroxene is shown at two fO_2 values (NNO and NNO + 3).

Crystallinity and phase proportions

At 200 MPa, the amount of crystals increases with decreasing water content and falling temperature (Fig. 3). At 950°C and ~5 wt % H_2O, the dacite is close to its liquidus with ~3 wt % of crystals; the highest crystal content (~50 wt %) was obtained at 950°C and 2·5 wt % H_2O, and at 850°C and 3·8 wt % H_2O. It should be noted that at 850°C (the temperature estimated from the Fe–Ti oxide equilibrium) and ~5–6 wt % H_2O, the crystallinity of the charges is 25–35 wt %, which is similar to the crystallinity of the dacitic lava (~30 wt %). Plagioclase and hornblende are the most abundant minerals in all S-free experiments, particularly below 925°C. Their proportions vary with temperature, water content, and fO_2. This is shown in Fig. 4, where we have plotted the plagioclase–hornblende ratio against the crystallinity of the experiment. For a given temperature, decreasing water content increases the plagioclase/hornblende value and the crystallinity. At 850°C, increasing the fO_2 from NNO to NNO + 3 increases the plagioclase/hornblende value and produces a small increase in the crystallinity. If we plot the crystallinity and plagioclase/hornblende value of the dacite we see that it best fits the experimental data at high water contents (~5·5 wt % H_2O), and at 850°C, NNO to

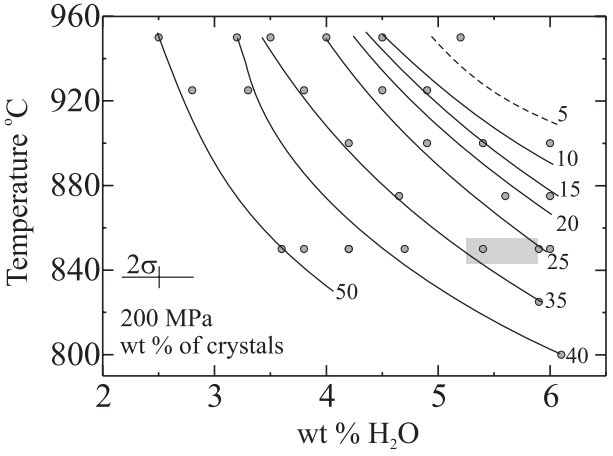

Fig. 3. Variation of crystallinity with temperature and water content for the San Pedro dacite at ~200 MPa. Grey box shows the crystallinity of the dacite lava at the temperature estimated from the Fe–Ti oxides, which suggests that the pre-eruptive water content in the melt was only about 5–6 wt %. Only S-free experiments have been used to construct the figure.

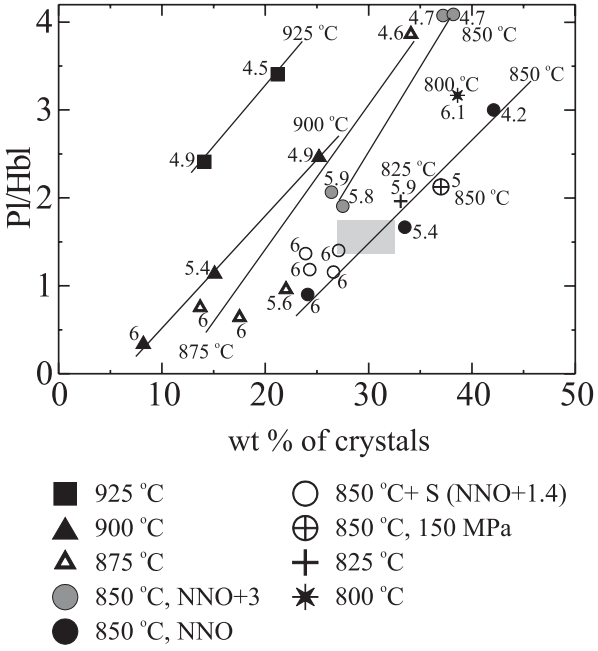

Fig. 4. Variation of the plagioclase/hornblende proportion (in wt %) with the crystallinity of the experimental charges. The lines are drawn through the data at a given temperature and show the effect of decreasing water contents (number next to the symbol). Grey box shows the data from the dacite lava. It should be noted that the Pl/Hbl and crystallinity values of the dacite are reproduced at high water contents (5·5–6 wt %) and 850°C, in accord with the pre-eruptive temperature estimated from the Fe–Ti oxides of the lava (850°C). Also included are the charges with 0·1–1 wt % added S run at 850°C and an fO_2 of NNO + 1·4, which contain biotite.

NNO + 1·4. Again, this is very close to the T–fO_2 conditions estimated from the Fe–Ti oxides in the lava. It should be noted that under water-saturated conditions at 150 MPa and NNO + 1 the experimental plagioclase/hornblende values and crystallinity are significantly higher than those of the lava, which suggests that the pre-eruptive pressure was probably not much lower than 200 MPa.

Phase compositions

Experimental glass compositions vary mainly according to temperature and water content (Table 4; Fig. 5), and range from dacitic at high temperature (950–925°C) and water contents (~5 wt %), to rhyolitic with up to 78 wt % SiO_2 and 4·7 wt % K_2O at 850°C and 3·5 wt % H_2O. The charges with the glass composition that best matches that of the glass inclusions or matrix glass of the lava, and that at the same time contain the mineral assemblage hornblende + plagioclase ± orthopyroxene, are those at 850°C and with 4·5–5·5 wt % H_2O (Fig. 5), in accord with the estimations made above from the phase proportions and crystallinity (e.g. Fig. 4).

Clinopyroxene at 950°C and 925°C is augitic ($Wo_{41-46}En_{47-43}Fs_{11-9}$), with ~4–5 wt % Al_2O_3 and *mg*-number of 79–83 (Table 5). These compositions are similar to those of the clinopyroxene found in the dacite, with the exception that those in the dacite have somewhat lower *mg*-number (74·6 ± 1·4) and Al_2O_3 content (1·7 ± 0·5 wt %). Orthopyroxene composition (Table 5) depends on temperature and fO_2. Charges run at high temperature (950–925°C) and fO_2 (NNO + 2·5 to NNO + 3·5) contain the orthopyroxene with the highest *mg*-number (up to 96). The *mg*-numbers of orthopyroxene from charges run at 850°C range from ~58 at NNO to 65 at NNO + 1 and water-saturated conditions (at 150 MPa), which are somewhat lower than the *mg*-number (71 ± 1) of orthopyroxene in the dacitic lava.

Experimental amphibole is magnesiohornblende or tschermakite [classification after Leake *et al.* (1997)] and its *mg*-number changes with temperature, but mainly with fO_2 (Table 6). The hornblende with the lowest *mg*-number (61 ± 2) is found in charges run at 850°C and NNO, whereas the highest is found in charges run at higher fO_2 (NNO + 3, *mg*-number ~74–85). The Al_2O_3 contents (8·3–10·9 wt %) appear mainly to vary with temperature but also with fO_2. High temperature and low fO_2 tend to promote high Al_2O_3 contents in hornblende. The *mg*-numbers of hornblende in the dacite range from 62 to 71, and Al_2O_3 contents from 7 to 10 wt %, which overlap with the values for experimental hornblendes crystallized at 850°C and NNO + 1·4 (*mg*-number 67–70; Al_2O_3 8·7–9·8 wt %). There are no significant differences between hornblende compositions crystallized at 150 MPa and those at 200 MPa. Hornblende crystallized at 405 MPa, 850°C, and water-saturated conditions has a somewhat higher Al_2O_3 content (11 ± 1 wt %) than that at 200 MPa for the same temperature. Biotite (Table 6)

Table 4: Experimental glass compositions (in wt %) normalized to 100% anhydrous

T (°C):	850	850	850	850	900	900	900	900
n:	19	17	2	3	11	10	10	11
Charge:	1	2	4	5	8	9	10	11
SiO_2	72·3(0·7)	73·9(0·3)	75·6(0·1)	76·9(0·7)	69·6(0·3)	71·0(0·2)	72·2(0·3)	73·9(0·8)
TiO_2	0·31(0·06)	0·29(0·06)	0·22(0·02)	0·25(0·02)	0·36(0·07)	0·42(0·05)	0·40(0·07)	0·38(0·04)
Al_2O_3	15·98(0·20)	14·95(0·23)	13·48(0·05)	12·76(0·11)	16·48(0·08)	15·77(0·14)	15·06(0·19)	14·10(0·21)
FeO*	2·02(0·38)	1·83(0·20)	1·45(0·12)	1·37(0·18)	2·27(0·18)	2·09(0·20)	1·94(0·19)	1·72(0·15)
MnO	0·09(0·08)	0·06(0·08)	0·15(0·02)	0·06(0·07)	0·06(0·05)	0·08(0·05)	0·08(0·07)	0·07(0·05)
MgO	0·30(0·14)	0·23(0·08)	0·24(0·07)	0·20(0·05)	0·96(0·07)	0·78(0·04)	0·67(0·03)	0·53(0·05)
CaO	2·42(0·14)	1·87(0·13)	1·39(0·05)	1·07(0·06)	3·58(0·13)	2·89(0·11)	2·37(0·11)	1·94(0·22)
Na_2O	3·77(0·25)	3·12(0·20)	3·05(0·05)	2·79(0·46)	4·30(0·15)	3·79(0·19)	3·82(0·14)	3·49(0·41)
K_2O	3·26(0·12)	3·67(0·12)	4·33(0·14)	4·55(0·16)	2·92(0·10)	3·16(0·11)	3·50(0·13)	3·89(0·06)
Total[1]	89·9(1·0)	90·1(1·0)	92·8(0·4)	93·4(1·4)	90·5(1·0)	91·5(0·7)	93·1(0·6)	93·7(1·0)
H_2O[2]	7·4	7·6	5·9	4·6	6·5	6·3	5·0	4·5
H_2O[3]	6·0	5·4	4·2	3·6	6·0	5·4	4·9	4·1

T (°C):	950	950	950	950	950	950	850	850
n:	7	7	10	8	10	8	9	10
Charge:	17	18	19	20	21	22	24	26
SiO_2	68·8(0·3)	69·8(0·7)	71·2(0·4)	73·1(0·2)	74·6(0·3)	75·8(0·4)	74·6(0·3)	76·1(0·3)
TiO_2	0·35(0·06)	0·42(0·09)	0·39(0·09)	0·30(0·08)	0·31(0·06)	0·28(0·08)	0·25(0·08)	0·23(0·08)
Al_2O_3	16·59(0·13)	16·10(0·17)	15·34(0·32)	14·33(0·18)	13·46(0·20)	12·78(0·23)	15·33(0·15)	13·49(0·12)
FeO*	1·76(0·06)	1·79(0·63)	1·64(0·17)	1·67(0·20)	1·49(0·18)	1·33(0·10)	0·77(0·11)	0·82(0·10)
MnO	0·06(0·09)	0·06(0·07)	0·10(0·09)	0·04(0·06)	0·06(0·07)	0·05(0·09)	0·04(0·05)	0·05(0·06)
MgO	1·56(0·06)	1·42(0·09)	1·06(0·07)	0·82(0·09)	0·59(0·05)	0·57(0·10)	0·49(0·05)	0·44(0·04)
CaO	3·97(0·16)	3·28(0·18)	2·88(0·17)	2·03(0·17)	1·56(0·10)	1·29(0·09)	2·06(0·10)	1·33(0·05)
Na_2O	4·01(0·09)	4·17(0·11)	4·15(0·16)	4·07(0·07)	3·89(0·11)	3·65(0·17)	3·21(0·22)	3·47(0·19)
K_2O	2·94(0·11)	2·97(0·22)	3·29(0·14)	3·60(0·15)	4·02(0·15)	4·21(0·16)	3·28(0·12)	4·06(0·15)
Total[1]	91·7(0·8)	92·1(0·5)	92·7(1·2)	94·5(0·4)	95·1(0·5)	95·1(0·9)	87·8(0·8)	92·2(0·8)
H_2O[2]	5·6	5·4	4·9	3·5	3·1	3·1	9·8	6·0
H_2O[3]	5·2	4·5	4·0	3·5	3·2	2·5	5·8	4·7

T (°C):	850	850	925	925	925	925	925
n:	8	4	8	7	8	7	5
Charge:	27	28	33	34	35	36	37
SiO_2	77·4(0·2)	78·2(0·2)	70·3(0·2)	71·7(0·3)	73·5(0·3)	74·9(0·3)	75·5(0·3)
TiO_2	0·21(0·08)	0·20(0·05)	0·39(0·12)	0·33(0·08)	0·37(0·09)	0·37(0·06)	0·40(0·06)
Al_2O_3	12·71(0·10)	11·98(0·12)	16·04(0·10)	15·50(0·18)	14·52(0·18)	13·87(0·21)	13·45(0·08)
FeO*	0·64(0·06)	0·82(0·05)	1·63(0·20)	1·48(0·32)	1·28(0·20)	1·15(0·19)	1·07(0·12)
MnO	0·10(0·08)	0·09(0·11)	0·04(0·03)	0·03(0·02)	0·06(0·05)	0·08(0·10)	0·03(0·04)
MgO	0·33(0·03)	0·26(0·02)	1·20(0·07)	1·06(0·05)	0·83(0·05)	0·65(0·03)	0·65(0·15)
CaO	1·01(0·09)	0·83(0·08)	3·35(0·12)	2·82(0·14)	2·06(0·12)	1·62(0·08)	1·40(0·11)
Na_2O	3·23(0·09)	2·86(0·11)	4·05(0·15)	3·82(0·19)	3·84(0·11)	3·48(0·14)	3·38(0·16)
K_2O	4·39(0·08)	4·72(0·13)	2·96(0·07)	3·27(0·12)	3·53(0·08)	3·86(0·11)	4·14(0·11)
Total[1]	93·5(0·4)	94·0(0·7)	91·9(0·9)	90·5(2·3)	93·1(0·5)	91·8(1·1)	92·9(1·1)
H_2O[2]	4·9	4·5	6·2	7·4	5·2	6·3	5·5
H_2O[3]	4·2	3·8	4·9	4·5	3·8	3·3	2·8

T (°C):	875	875	875	900	900	875	875	875
n:	10	9	7	10	7	5	4	4
Charge:	40	41	46cr	47	51s	81s	86	87s
SiO_2	72·0(0·2)	73·3(0·5)	70·9(0·4)	71·0(0·3)	71·7(0·2)	70·7(0·2)	71·3(0·2)	70·9(0·5)
TiO_2	0·36(0·10)	0·33(0·08)	0·40(0·07)	0·37(0·05)	0·46(0·04)	0·29(0·02)	0·28(0·02)	0·36(0·05)
Al_2O_3	16·20(0·15)	15·78(0·23)	16·04(0·18)	16·89(0·09)	16·70(0·15)	17·21(0·15)	16·34(0·13)	16·40(0·55)
FeO*	1·68(0·19)	1·30(0·16)	2·25(0·21)	1·79(0·26)	1·44(0·11)	0·82(0·05)	1·19(0·08)	0·87(0·02)
MnO	0·05(0·06)	0·06(0·05)	0·03(0·05)	0·06(0·04)	0·06(0·05)	0·06(0·03)	0·06(0·01)	0·09(0·07)
MgO	0·31(0·11)	0·20(0·07)	0·67(0·05)	0·18(0·05)	0·26(0·06)	1·37(0·03)	0·83(0·03)	1·21(0·02)
CaO	2·81(0·17)	2·50(0·10)	2·89(0·09)	3·09(0·09)	2·88(0·15)	2·36(0·04)	2·85(0·09)	2·71(0·07)
Na_2O	4·14(0·18)	3·19(0·26)	4·32(0·12)	3·95(0·13)	3·57(0·15)	4·60(0·07)	4·42(0·10)	4·65(0·08)
K_2O	3·00(0·08)	3·34(0·09)	3·05(0·15)	3·00(0·08)	3·10(0·07)	2·89(0·06)	3·16(0·12)	3·13(0·06)
Total[1]	88·1(1·2)	86·6(1·0)	89·1(0·4)	90·2(0·8)	89·8(0·9)	93·5(0·4)	92·9(0·4)	92·8(0·5)
S (ppm)						381(28)		377(27)
H_2O[2]	9·1	10·8	8·1	6·4	6·8	6·0	6·0	6·1
H_2O[3]	6·0	5·6	6·0	6·0	6·0	6·0	6·0	6·0

T (°C):	875	850	850	850	850	875	875	800
n:	4	7	9	5	5	8	9	6
Charge:	88s	89s	94	95s	96s	97	98s	108
SiO_2	70·9(0·2)	73·0(0·4)	72·9(0·2)	73·4(0·3)	73·4(0·1)	70·1(0·2)	71·1(0·2)	75·3(0·2)
TiO_2	0·29(0·05)	0·36(0·03)	0·35(0·03)	0·33(0·04)	0·37(0·02)	0·38(0·03)	0·47(0·03)	0·19(0·03)
Al_2O_3	16·45(0·10)	16·03(0·10)	16·04(0·11)	16·02(0·15)	16·07(0·09)	16·21(0·09)	16·07(0·08)	14·33(0·12)
FeO*	1·21(0·08)	1·44(0·15)	1·39(0·20)	1·16(0·18)	0·96(0·17)	2·78(0·19)	1·80(0·09)	0·83(0·09)
MnO	0·08(0·03)	0·05(0·06)	0·06(0·03)	0·05(0·05)	0·07(0·03)	0·05(0·03)	0·08(0·04)	0·09(0·05)
MgO	0·93(0·04)	0·35(0·09)	0·24(0·08)	0·24(0·04)	0·15(0·05)	0·71(0·03)	0·70(0·03)	0·36(0·02)
CaO	2·78(0·03)	1·97(0·15)	2·18(0·07)	1·92(0·08)	2·01(0·06)	2·92(0·07)	2·73(0·08)	1·57(0·07)
Na_2O	4·51(0·07)	3·57(0·15)	3·67(0·08)	3·47(0·10)	3·47(0·10)	4·33(0·10)	4·35(0·05)	3·96(0·14)
K_2O	3·21(0·07)	3·51(0·08)	3·50(0·09)	3·57(0·06)	3·62(0·07)	3·10(0·07)	3·23(0·06)	3·88(0·06)
Total[1]	93·3 (0·2)	90·8 (0·5)	91·1 (0·6)	90·0 (0·5)	90·2 (0·4)	92·1 (0·5)	91·5 (0·5)	91·9 (0·5)
S (ppm)	333 (30)	324 (18)		355 (30)	322 (40)		180 (26)	
H_2O[2]	6·2	7·5	7·4	8·4	8·2	6·0	6·4	6·2
H_2O[3]	6·0	5·9	5·9	5·9	5·9	6·0	6·0	6·1

T (°C):	800	825	825	850	850	850	850	850
n:	5	10	7	7	7	4	7	7
Charge:	109s	133	137s	141cr	142	143	144s	146s
SiO_2	75·3(0·1)	74·6(0·4)	74·0(0·3)	73·1(0·3)	73·9(0·2)	76·2(0·3)	73·5(0·2)	73·5(0·2)
TiO_2	0·11(0·04)	0·29(0·04)	0·31(0·04)	0·20(0·03)	0·27(0·03)	0·21(0·02)	0·38(0·04)	0·29(0·04)
Al_2O_3	15·17(0·08)	15·47(0·12)	15·12(0·08)	15·78(0·04)	15·60(0·10)	13·87(0·14)	16·94(0·14)	16·37(0·11)
FeO*	0·77(0·11)	1·54(0·09)	1·50(0·10)	0·92(0·10)	0·96(0·05)	0·86(0·14)	0·40(0·08)	0·57(0·05)
MnO	0·05(0·03)	0·05(0·04)	0·08(0·07)	0·05(0·05)	0·03(0·04)	0·04(0·04)	0·08(0·03)	0·07(0·04)
MgO	0·67(0·04)	0·42(0·03)	0·47(0·02)	0·59(0·06)	0·55(0·06)	0·41(0·07)	0·85(0·08)	0·98(0·04)
CaO	1·36(0·05)	1·96(0·09)	1·92(0·09)	2·20(0·07)	2·19(0·07)	1·43(0·11)	1·92(0·08)	1·85(0·04)
Na_2O	4·00(0·09)	3·67(0·13)	3·71(0·17)	4·31(0·09)	3·62(0·14)	3·12(0·17)	3·71(0·18)	4·10(0·09)
K_2O	3·08(0·09)	3·46(0·15)	3·37(0·08)	3·44(0·07)	3·40(0·09)	3·89(0·08)	2·78(0·07)	2·84(0·06)
Total[1]	92·8(0·4)	90·5(0·9)	89·9(0·7)	91·7(0·5)	89·6(0·9)	90·0(1·5)	88·3(0·7)	90·4(0·6)
S (ppm)	150 (50)		270 (20)				308 (45)	267 (52)
H_2O[2]	6·0	8·9	9·4	7·2	9·4	8·9	10·6	8·6
H_2O[3]	6·1	5·9	5·9	6·0	6·0	3·3	6·0	6·0

Table 4: Continued

T (°C):	850	850	850	875
n:	7	6	1	7
Charge:	148s	184	186	201
SiO_2	73·6(0·3)	74·1(0·4)	76·9	74·5(0·4)
TiO_2	0·20(0·03)	0·32(0·04)	0·28	0·25(0·04)
Al_2O_3	16·33(0·10)	14·80(0·11)	13·9	14·63(0·11)
FeO*	0·75(0·06)	1·65(0·09)	1·04	1·06(0·16)
MnO	0·09(0·04)	0·08(0·04)	0·01	0·07(0·05)
MgO	0·91(0·09)	0·34(0·05)	0·13	0·60(0·05)
CaO	2·05(0·04)	1·59(0·12)	1·06	1·64(0·07)
Na_2O	3·83(0·14)	3·10(0·1)	2·47	3·32(0·27)
K_2O	2·77(0·08)	4·02(0·06)	4·31	3·94(0·14)
Total[1]	89·5(0·6)	90·5(0·8)	90·9	91·3(1·1)
S (ppm)	286(34)			
H_2O[2]	9·5	8·3	7·8	8·3
H_2O[3]	6·0	4·9	3·9	4·7

*Total iron as Fe^{2+}.
[1]Original total.
[2]Water estimated with the by-difference method (see text for details).
[3]Water estimated by mass-balance and the solubility model of Tamic *et al.* (2001; see text for details).
n, number of electron microprobe analyses. Numbers in parentheses are the 2σ deviations from the mean. The letter 's' after the charge number indicates that S was added to the starting material, whereas the letters 'cr' indicate that the starting material is the crushed rock.

crystallized at high oxygen fugacities (∼NNO + 3) and thus it has a high *mg*-number (∼84).

Plagioclase compositions (Table 7) range from An_{64} at 900°C and water-saturated conditions down to An_{32} at 825°C and low water contents (∼4·5 wt %). This variation spans the whole compositional range of plagioclase crystals in the dacite (An_{65-35}), except for the xenocrysts at An_{84-82}. High temperatures and high water contents promote high An contents in plagioclase (Fig. 6). The rims of plagioclase phenocrysts in the dacitic lava are An_{40-35}, which at 850°C and 200 MPa constrains the water content to be 4·5–5·5 wt %, in accord with the observations made above for the glass composition, crystallinity, and phase proportions.

Titanomagnetite was very difficult to analyse because of its small size, and in many cases the calculated total after estimating the Fe_2O_3/FeO proportions with the structural formula [calculated as done by Stormer (1983)] are lower than 100% (Table 8). Titanomagnetites have ulvöspinel contents that range from 0·08 to 0·39. For a given temperature, the Ti content of titanomagnetite increases with decreasing fO_2.

Phase relations, proportions, and composition of S-bearing charges

In experiments with 1 wt % of added S, biotite is part of the mineral assemblage at $fO_2 \geq$ NNO + 1·4 and temperatures ≤875°C (Fig. 7). At moderate fO_2 (e.g. NNO + 1·4) biotite coexists with plagioclase, hornblende, anhydrite plus pyrrhotite, whereas at high fO_2 (e.g. NNO + 3) hornblende disappears, and biotite coexists with plagioclase and anhydrite only. This suggests that at NNO + 3 anhydrite crystallization tends to destabilize hornblende and this, in turn, enhances biotite stability up to 875°C (see also below). The stabilities of biotite and hornblende also appear to depend on the amount of S added. Biotite is present at 850 and 875°C, with $fO_2 \geq$ NNO + 1·4 and with 0·5 and 1 wt % S, but disappears at both temperatures when we added only 0·1 wt % S (Fig. 7), whereas hornblende is absent in charges with 1 wt % added S at 800–875°C and an fO_2 of ∼NNO + 3.

The crystallinity and phase proportions of S-bearing experiments are also appreciably different from those for S-free experiments, particularly at high fO_2 (e.g. NNO + 3). At 850°C and 875°C and at NNO + 3 the charges with 1 wt % of added S have ∼10 wt % more glass than the S-free charges, which is mainly due to lower plagioclase proportions in S-bearing experiments (Table 3). These effects tend to disappear with decreasing amounts of added S. At lower fO_2 (NNO + 1·4) the differences in the phase proportions between the S-free and S-bearing experiments are much smaller, apart from the presence of S-bearing minerals and biotite (e.g. compare charges 89 s and 94 in Table 3).

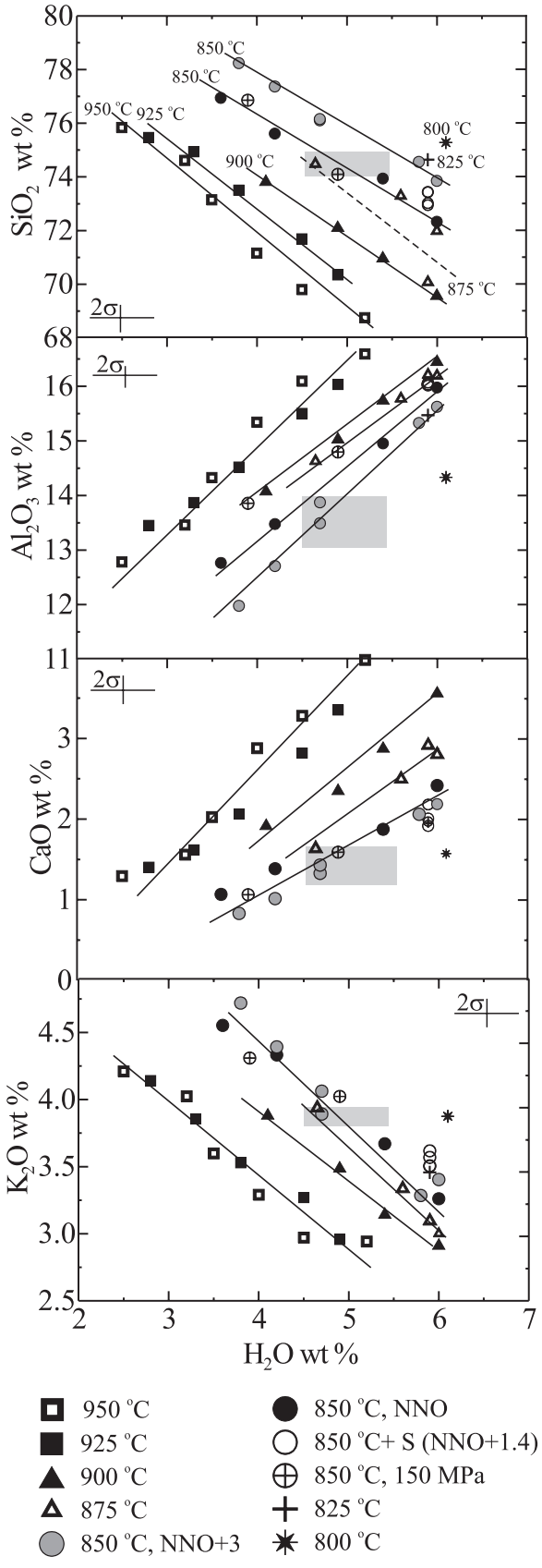

Despite these effects on the phase equilibria and mineral proportions, there are no significant differences between phase compositions (glass, hornblende and plagioclase) in S-bearing and S-free charges run at about the same P–T–$f\,H_2O$–fO_2 conditions (Tables 4, 6, and 7). The S contents of the glasses in the S-bearing experiments are higher in charges run at high temperature and high fO_2, and range from ~380 ppm at 875°C and NNO + 3 to about 150 ppm at 800°C. For comparison, the S contents of the glass inclusions in phenocrysts in the dacite are ~300 ppm. The *mg*-numbers of biotite (Table 6) vary with fO_2, from ~93 at NNO + 3 to ~70 at NNO + 1·4, the lower values approaching those of biotites in the dacitic lava (60–67).

DISCUSSION

The effect of S on phase equilibria, phase proportions, and compositions

There are very few previous studies that provide information concerning the effects of S on phase equilibria in hydrous magmas; the majority of previous S-bearing experimental studies were designed to determine S solubility, particularly at low oxygen fugacities and dry conditions [e.g. the review by Carroll & Webster (1994)]. The work of Scaillet & Evans (1999) on the Pinatubo dacite explored to a limited extent the consequences of addition of minor quantities of S (1 wt % S, added as elemental S) in oxidized and water-rich systems. In their experiments performed at fO_2 > NNO + 2, where anhydrite was stable, they found similar effects on the phase equilibria to those reported here, including an increase in biotite stability (which was present only in S-bearing charges), and the destabilization of hornblende, which at the temperature at which the experiments were performed (781°C) was replaced by gedrite. The increase in the proportion of glass and decrease in the amount of plagioclase in S-bearing charges that we report were also observed in the experiments of Scaillet & Evans (1999) with ~1 wt % of added S at $fO_2 \geq$ NNO + 1·7. S-bearing charges contain about 3–10 wt % more glass than those that are S-free, typically because of a decrease in the plagioclase proportion [e.g. charges 65 and 69 of Scaillet & Evans (1999)]. Although the role of S in the silicate melt structure is virtually unknown, particularly at high fO_2 (e.g. >NNO + 1·5) and hydrous conditions, the increased melt fraction and the lower plagioclase proportion in S-bearing charges could be due to the presence of Ca–SO_4 complexes in the melt, by analogy

Fig. 5. Variation of glass composition with temperature and water content. The charges with the glass composition that best matches that of the glass inclusions or matrix glass of the lava (grey box) are those at 850°C and with 5 ± 0·5 wt % H_2O, in accord with the estimations made from the phase proportions and crystallinity (Fig. 4). Also included are the charges with 0·1–1 wt % added S run at 850°C and an fO_2 of NNO + 1·4, which contain biotite.

Table 5: Experimental pyroxene compositions (in wt %)

Mineral:	Opx	Opx	Opx	Opx	Opx	Opx	Opx	Opx
T (°C):	850	850	900	950	950	925	925	850
n:	8	5	10	3	2	1	1	9
Charge:	2	4	11	20	21	35	36	184
SiO_2	51·1(0·5)	50·7(0·3)	54·0(0·4)	56·6(0·5)	57·0(0·4)	56·4	56·4	51·5(0·5)
TiO_2	0·25(0·10)	0·30(0·16)	0·30(0·09)	0·15(0·04)	0·11(0·05)	0·18	0·16	0·21(0·02)
Al_2O_3	1·62(0·29)	1·98(0·58)	1·89(0·23)	1·98(0·43)	2·02(0·28)	2·69	2·72	1·86(0·25)
FeO*	24·4(0·4)	26·4(0·6)	14·54(0·55)	5·20(0·58)	5·44(0·19)	2·64	2·33	20·5(0·3)
MnO	0·71(0·14)	0·60(0·14)	0·69(0·08)	0·62(0·08)	0·76(0·16)	0·26	0·27	0·83(0·05)
MgO	19·2(0·2)	16·4(0·4)	25·9(0·3)	32·9(0·8)	32·2(0·4)	35·5	35·1	21·4(0·3)
CaO	1·31(0·27)	1·88(0·13)	1·62(0·17)	1·26(0·17)	1·24(0·17)	1·22	1·11	1·16(0·14)
Sum	98·7(0·5)	98·6(0·3)	99·0(0·6)	98·8(0·3)	99·0(0·5)	98·9	98·2	97·7(0·6)
Wo	2·8(0·6)	4·1(0·3)	3·3(0·4)	2·5(0·3)	2·4(0·3)	2·3	2·1	2·4(0·3)
En	56·1(0·6)	49·9(0·4)	72·7(0·4)	88·7(1·2)	88·1(0·3)	93·4	94·0	62·5(0·3)
Fs	41·2(0·4)	46·0(0·3)	24·0(0·7)	8·8(0·9)	9·5(0·6)	4·3	3·9	35·0(0·3)
mg-no.	58·4(0·4)	52·6(0·4)	76·1(0·6)	91·8(1·0)	91·4(0·4)	96·0	96·4	65·0(0·3)

Mineral:	Cpx	Cpx	Cpx	Cpx	Cpx	Cpx
T (°C):	950	950	950	950	925	925
n:	4	2	2	1	1	1
Charge:	17	18	19	21	33	35
SiO_2	50·7(0·4)	50·6(0·3)	51·3(0·4)	52·4(1·2)	51·2	51·3
TiO_2	0·60(0·09)	0·61(0·07)	0·43(0·07)	0·45(0·11)	0·65	0·61
Al_2O_3	4·85(0·68)	5·29(0·23)	4·22(0·36)	3·80(0·32)	5·69	4·68
FeO*	6·08(0·27)	6·62(0·12)	5·74(0·37)	6·35(0·61)	5·37	5·91
MnO	0·24(0·04)	0·32(0·04)	0·40(0·03)	0·41(0·02)	0·25	0·22
MgO	14·33(0·37)	14·23(0·50)	15·26(0·34)	15·69(0·04)	14·94	14·04
CaO	20·8(0·9)	20·1(0·6)	21·0(0·2)	19·0(0·4)	21·4	20·9
Na_2O	0·63(0·10)	0·67(0·06)	0·63(0·04)	0·81(0·08)	0·75	0·90
Sum	98·3(0·4)	98·5(0·4)	99·0(0·3)	98·9(0·4)	99·9	98·6
Wo	45·6(0·9)	44·3(0·1)	44·6(0·4)	41·2(0·1)	46·6	46·3
En	43·6(0·3)	43·7(0·4)	45·2(0·7)	47·4(0·9)	43·9	43·2
Fs	10·8(0·7)	12·0(0·6)	10·2(0·7)	11·4(0·8)	9·5	10·6
mg-no.	80·8(1·1)	79·3(0·9)	82·6(1·2)	81·5(1·4)	82·8	80·9

*Total iron as Fe^{2+}.
Wo = 100Ca/(Ca + Fe* + Mg); En = 100Mg/(Mg + Ca + Fe*); Fs = 100Fe*/(Fe* + Ca + Mg); *mg*-number = 100Mg/(Mg + Fe*); *n*, number of electron microprobe analyses. Numbers in parentheses as in Table 4.

with the Fe–S complexes that have been proposed at much more reducing conditions (e.g. Carroll & Webster, 1994). Scaillet & Evans (1999) did not find any significant change in the mineral compositions in experiments performed at $fO_2 > NNO + 1{\cdot}7$, but they noted an increase in the *mg*-number of hornblende at lower fO_2 (e.g. NNO to NNO + 1) in S-bearing charges that contained pyrrhotite. Because biotites from the lava contain up to 170 ppm S, the effect of S on biotite stability could be perhaps due to the substitution of HS^- for OH^- in the biotite structure. An increase in the *mg*-number of hornblende and biotite in S-bearing charges was also found in early experimental studies using compositions made of biotite, amphibole, and pyrrhotite mixtures and with fO_2 at ~NNO − 0·4 (e.g. Popp *et al.*, 1977; Tso *et al.*, 1979). In the present study we did not conduct any S-bearing experiments at $fO_2 < NNO + 1{\cdot}2$, thus our experimental results are not able to address this issue.

Table 6: Experimental hornblende and biotite (or phlogopite) compositions (in wt %)

Mineral:	Hbl	Hbl	Hbl	Hbl	Hbl	Hbl	Hbl	Hbl
T (°C):	850	850	900	900	900	850	850	925
n:	9	7	4	5	12	7	10	9
Charge:	1	2	8	9	0	24	26	33
SiO_2	47·1(1·1)	47·5(1·3)	44·4(0·6)	45·2(0·3)	45·1(0·3)	47·7(1·3)	47·9(0·4)	46·0(0·7)
TiO_2	1·81(0·24)	1·87(0·27)	1·62(0·11)	1·88(0·14)	2·09(0·13)	1·53(0·19)	1·14(0·11)	1·23(0·05)
Al_2O_3	10·87(0·29)	10·19(1·00)	10·78(0·15)	10·25(0·11)	9·50(0·18)	10·02(0·55)	8·49(0·56)	9·97(0·43)
FeO*	13·04(0·75)	13·18(0·79)	10·08(0·16)	10·20(0·28)	9·78(0·35)	8·80(0·79)	5·85(0·39)	6·05(0·33)
MnO	0·23(0·10)	0·30(0·09)	0·16(0·09)	0·16(0·09)	0·22(0·11)	0·21(0·08)	0·37(0·08)	0·26(0·08)
MgO	11·53(0·57)	11·85(1·18)	14·74(0·15)	15·07(0·54)	15·39(0·28)	14·12(0·43)	18·01(0·54)	17·64(0·50)
CaO	9·93(0·56)	9·37(0·43)	11·65(0·18)	10·85(0·37)	11·21(0·25)	10·58(0·44)	11·72(0·21)	11·82(0·31)
Na_2O	1·92(0·18)	1·90(0·24)	2·06(0·06)	1·97(0·07)	1·89(0·08)	1·94(0·15)	1·70(0·11)	1·90(0·10)
K_2O	0·81(0·16)	0·71(0·16)	0·62(0·02)	0·56(0·08)	0·53(0·05)	0·61(0·08)	0·49(0·03)	0·55(0·06)
Sum	97·4(0·5)	96·9(0·4)	96·1(0·5)	96·1(0·3)	95·7(0·7)	95·5(0·9)	95·7(0·5)	95·4(0·9)
mg-no.	61·2(1·9)	61·5(1·7)	72·3(0·2)	72·5(1·1)	73·7(0·6)	74·1(2·1)	84·5(0·9)	83·8(1·0)

Mineral:	Hbl	Hbl	Hbl	Hbl	Hbl	Hbl	Hbl	Hbl
T (°C):	925	875	875	875	900	900	850	850
n:	8	10	5	6	7	6	11	6
Charge:	34	40	41	46cr	47	51s	67	71
SiO_2	46·3(0·5)	45·2(0·8)	46·1(0·4)	46·1(1·6)	45·3(0·7)	48·2(1·1)	44·5(1·5)	43·9(0·5)
TiO_2	1·29(0·06)	2·00(0·18)	1·84(0·12)	1·69(0·51)	1·92(0·12)	1·82(0·15)	1·59(0·17)	1·43(0·12)
Al_2O_3	9·45(0·43)	9·70(0·66)	10·36(0·21)	7·86(1·95)	10·31(0·44)	11·0(0·63)	11·03(1·06)	9·91(0·71)
FeO*	5·69(0·21)	12·38(0·40)	10·65(0·36)	12·63(1·34)	11·34(0·38)	9·47(0·40)	13·18(1·13)	12·70(0·29)
MnO	0·24(0·08)	0·19(0·05)	0·29(0·03)	0·32(0·19)	0·19(0·05)	0·26(0·06)	0·27(0·08)	0·27(0·07)
MgO	18·03(0·32)	12·95(0·66)	13·60(0·52)	14·01(0·43)	14·45(0·63)	12·88(1·10)	11·49(1·31)	14·22(0·42)
CaO	11·80(0·18)	10·64(1·08)	10·67(0·23)	10·72(0·38)	11·10(0·26)	10·14(0·51)	10·01(0·76)	10·05(0·27)
Na_2O	1·83(0·09)	1·87(0·17)	1·95(0·05)	1·64(0·39)	1·91(0·10)	1·93(0·17)	1·97(0·15)	1·70(0·04)
K_2O	0·51(0·06)	0·47(0·08)	0·55(0·08)	0·45(0·11)	0·55(0·07)	0·77(0·10)	0·78(0·26)	0·40(0·03)
Sum	95·1(0·8)	95·4(0·4)	96·0(0·5)	95·4(0·9)	97·1(0·5)	96·8(0·7)	94·8(0·9)	94·7(0·5)
mg-no.	85·0(0·6)	65·1(0·8)	69·5(1·0)	66·5(2·9)	69·4(1·5)	70·7(1·6)	60·8(1·9)	66·6(1·1)

Mineral:	Hbl	Hbl	Hbl	Hbl	Hbl	Hbl	Hbl	Hbl
T (°C):	875	875	850	850	850	850	875	875
n:	4	5	6	6	3	5	7	7
Charge:	86	88s	89s	94	95s	96s	97	98s
SiO_2	46·6(0·2)	45·6(1·0)	45·5(1·3)	44·8(0·9)	45·5(0·6)	45·4(0·9)	44·9(0·8)	45·8(0·8)
TiO_2	1·36(0·07)	1·79(0·17)	1·68(0·07)	1·62(0·22)	1·70(0·08)	1·79(0·10)	1·74(0·10)	1·88(0·10)
Al_2O_3	9·21(0·45)	10·28(0·44)	8·73(1·13)	9·82(0·38)	9·27(0·57)	9·79(0·31)	9·98(0·35)	9·06(0·64)
FeO*	9·05(0·33)	9·82(0·52)	11·73(0·07)	11·47(0·44)	12·21(0·16)	12·16(0·55)	11·46(0·46)	11·24(0·35)
MnO	0·20(0·05)	0·20(0·02)	0·40(0·03)	0·26(0·04)	0·34(0·04)	0·27(0·04)	0·26(0·08)	0·24(0·06)
MgO	16·34(0·50)	15·57(0·44)	15·37(0·58)	14·53(0·45)	14·62(0·59)	13·92(0·61)	14·68(0·42)	15·66(0·31)
CaO	11·63(0·87)	11·11(0·24)	10·73(0·16)	10·58(0·36)	10·31(0·09)	10·32(0·57)	11·34(0·60)	10·45(0·24)
Na_2O	1·77(0·09)	2·03(0·04)	1·63(0·19)	1·93(0·07)	1·76(0·11)	1·85(0·08)	1·96(0·15)	1·73(0·08)
K_2O	0·49(0·05)	0·54(0·03)	0·38(0·04)	0·55(0·06)	0·53(0·12)	0·62(0·14)	0·51(0·06)	0·40(0·02)
Sum	96·8(0·7)	97·0(0·2)	96·4(0·2)	95·5(0·4)	96·3(0·3)	96·1(0·2)	96·9(0·9)	96·4(0·6)
mg-no.	76·3(1·2)	73·9(1·6)	70·0(0·9)	69·3(0·7)	68·1(0·9)	67·1(1·0)	69·5(1·3)	71·3(0·8)

Table 6: Continued

Mineral:	Hbl	Hbl	Hbl	Hbl	Hbl	Hbl	Hbl	Hbl
T (°C):	800	825	825	850	850	850	850	875
n:	4	4	4	13	7	6	8	6
Charge:	108	133	137s	141cr	142	143	184	201
SiO_2	48·7(1·1)	47·1(1·1)	46·5(0·5)	45·3(1·8)	46·6(0·4)	48·9(0·9)	44·8(1·6)	47·6(0·9)
TiO_2	0·87(0·09)	1·58(0·12)	1·69(0·13)	1·60(0·75)	1·44(0·15)	1·10(0·05)	2·08(0·16)	1·09(0·10)
Al_2O_3	8·77(0·82)	9·48(0·67)	8·33(0·27)	9·09(1·07)	9·76(0·27)	8·11(0·53)	9·33(0·26)	8·85(0·75)
FeO*	9·25(0·36)	11·70(0·72)	11·93(0·48)	10·09(2·90)	8·65(0·82)	5·88(0·69)	13·41(0·59)	5·18(0·32)
MnO	0·40(0·02)	0·31(0·05)	0·45(0·04)	0·30(0·06)	0·30(0·06)	0·30(0·09)	0·22(0·04)	0·32(0·04)
MgO	15·29(0·53)	13·44(0·97)	14·64(0·54)	15·80(2·32)	15·41(0·75)	18·54(0·87)	12·79(0·57)	18·82(0·63)
CaO	11·43(1·31)	10·06(0·67)	10·76(0·26)	11·20(0·45)	11·21(0·40)	11·49(0·35)	9·95(0·47)	11·85(0·27)
Na_2O	1·42(0·15)	1·65(0·11)	1·42(0·08)	1·81(0·28)	1·81(0·08)	1·60(0·08)	1·88(0·06)	1·80(0·13)
K_2O	0·56(0·13)	0·62(0·18)	0·35(0·03)	0·47(0·07)	0·49(0·06)	0·51(0·09)	0·64(0·13)	0·50(0·07)
Sum	96·7(0·6)	95·9(0·6)	96·1(0·7)	95·7(0·9)	95·7(0·5)	96·4(0·2)	95·1(0·7)	96·0(0·5)
mg-no.	74·6(1·0)	67·2(1·4)	68·6(1·4)	73·4(8·4)	76·0(2·6)	84·9(1·9)	63·0(1·1)	86·6(1·1)
Mineral:	Bt	Bt	Bt	Bt	Bt	Bt	Bt	Bt
T (°C):	875	875	850	800	825	850	850	850
n:	5	5	2	1	6	4	4	4
Charge:	81s	87s	89s	108r	137s	144s	146s	148s
SiO_2	40·6(1·1)	40·7(0·6)	40·9(0·7)	39·3	44·5(1·5)	41·4(1·3)	40·9(0·8)	43·6(1·1)
TiO_2	2·96(0·53)	2·97(0·23)	3·67(0·18)	2·38	3·18(0·17)	3·48(0·18)	2·85(0·53)	2·11(0·26)
Al_2O_3	15·82(0·06)	15·37(0·07)	14·63(0·21)	14·8	15·03(0·35)	15·99(0·19)	16·16(0·24)	15·65(0·19)
FeO*	4·14(0·43)	3·02(0·19)	11·08(0·07)	7·00	10·19(0·58)	3·49(1·29)	3·78(0·83)	4·52(0·45)
MnO	0·09(0·06)	0·12(0·03)	0·10(0·03)	0·16	0·08(0·04)	0·07(0·01)	0·09(0·03)	0·11(0·04)
MgO	22·19(0·95)	22·96(0·29)	15·08(0·41)	21·3	13·92(0·97)	20·59(0·33)	20·29(0·74)	18·80(0·58)
CaO	0·09(0·10)	0·10(0·06)	0·26(0·05)	0·07	0·34(0·05)	0·13(0·06)	0·14(0·05)	0·26(0·04)
Na_2O	1·34(0·07)	1·26(0·08)	1·06(0·02)	0·30	1·15(0·05)	1·24(0·06)	1·26(0·03)	1·29(0·05)
K_2O	7·68(0·23)	7·73(0·09)	7·61(0·15)	8·26	7·29(0·33)	7·46(0·14)	7·39(0·17)	7·09(0·16)
Sum	94·9(0·2)	94·2(0·9)	94·5(0·5)	93·5	95·7(1·1)	93·9(0·6)	92·8(1·5)	93·5(0·7)
mg-no.	90·6(0·6)	93·1(0·4)	70·8(0·4)	84·4	70·9(0·5)	91·4(2·9)	90·5(2·1)	88·1(0·9)

*Total iron as Fe^{2+}.
mg-number = 100Mg/(Mg + Fe*). *n*, number of electron microprobe analyses. Numbers in parentheses as in Table 4. The letter 's' after the charge number indicates that S was added to the starting material; the letters 'cr' indicate that the starting material is the crushed rock; the letter 'r' indicates a mineral that was recalculated by subtracting glass.

Other S-bearing experimental studies that have been carried out on silicic hydrous compositions and at high fO_2, and thus are pertinent for comparison with our results, are those of Carroll & Rutherford (1985, 1987) for the Mount St. Helens dacite and El Chichón trachyandesite, and that of Luhr (1990) for the El Chichón trachyandesite. In the experiments of Carroll & Rutherford (1985, 1987) relatively large amounts of S were added to the starting composition in the form of pyrrhotite (3–10 wt %) or anhydrite (3 wt %); direct comparison of S-bearing and S-free experimental results is not possible because adding such an amount of S-bearing minerals changed significantly the starting bulk composition, and thus any changes in the phase equilibria, proportions or compositions cannot be interpreted to be the result of S addition only. In the experiments of Luhr (1990) relatively low amounts of S were added either as pyrrhotite or as anhydrite depending on the fO_2, with bulk S contents of ~1·2 wt %, similar to the highest amount of S added in our experiments. Although comparison of S-free and S-bearing experimental results for El Chichón is not possible because no S-free experiments were reported, Luhr (1990) investigated the effect of fO_2, at NNO − 0·4, NNO + 3·6, and NNO + 4·4,

Table 7: Experimental plagioclase compositions (in wt %)

T (°C):	850	850	900	900	950	950	950	950
n:	3	3	6	1	7	5	2	2
Charge:	1	2	8	11	18	19	20	21
SiO_2	57·8(0·3)	58·2(0·6)	51·8(0·7)	56·8	53·5(0·3)	58·0(0·8)	57·7(0·6)	60·8(0·1)
Al_2O_3	25·7(0·3)	25·3(0·2)	29·4(0·3)	26·0	27·6(0·3)	24·2(0·4)	24·8(1·2)	22·5(0·1)
FeO*	0·72(0·09)	0·75(0·18)	0·77(0·10)	0·85	1·05(0·13)	1·19(0·13)	1·05(0·05)	1·27(0·10)
MgO	0·08(0·02)	0·07(0·02)	0·06(0·02)	0·14	0·16(0·13)	0·34(0·03)	0·22(0·04)	0·29(0·02)
CaO	8·82(0·15)	7·99(0·44)	12·93(0·39)	9·22	11·72(0·29)	8·73(0·22)	9·20(0·46)	7·12(0·03)
Na_2O	5·78(0·23)	6·27(0·22)	3·84(0·14)	5·43	4·49(0·12)	4·37(0·12)	4·80(0·09)	4·96(0·03)
K_2O	0·49(0·05)	0·52(0·06)	0·21(0·04)	0·52	0·30(0·05)	1·02(0·08)	0·85(0·17)	1·36(0·05)
Sum	99·5(0·7)	99·2(0·2)	99·1(0·7)	98·9	98·9(0·6)	97·9(0·8)	98·7(0·9)	98·4(0·2)
An	44·4(0·8)	40·0(1·8)	64·2(1·5)	46·9	58·0(0·8)	48·9(0·5)	48·7(1·3)	40·2(0·2)
Ab	52·6(1·0)	56·9(2·0)	34·6(1·3)	50·0	40·2(0·8)	44·3(0·5)	45·9(0·2)	50·7(0·2)
Or	3·0(0·4)	3·1(0·4)	1·3(0·2)	3·2	1·8(0·3)	6·8(0·6)	5·4(1·2)	9·2(0·2)

T (°C):	850	850	925	925	925	925	875	875
n:	1	1	9	9	14	4	7	4
Charge:	26r	28r	34	35	36	37	40	46cr
SiO_2	57·8	59·8	56·5(0·9)	57·2(0·9)	57·9(0·8)	58·1(0·5)	53·8(0·5)	54·1(1·6)
Al_2O_3	25·8	24·1	24·7(0·8)	24·2(0·8)	23·7(1·1)	23·1(1·3)	28·0(0·2)	28·1(1·3)
FeO*	0·83	0·99	1·00(0·13)	1·23(0·22)	1·04(0·14)	1·22(0·18)	0·59(0·04)	0·50(0·08)
MgO	0·12	0·49	0·20(0·06)	0·29(0·30)	0·12(0·10)	0·23(0·17)	0·04(0·03)	0·05(0·03)
CaO	8·53	7·31	9·19(0·47)	8·39(0·57)	7·68(0·47)	7·16(0·50)	11·42(0·35)	7·12(0·03)
Na_2O	6·26	6·30	4·84(0·22)	5·47(0·41)	5·75(0·28)	5·94(0·21)	4·56(0·25)	4·82(0·32)
K_2O	0·50	0·94	0·60(0·09)	0·55(0·06)	0·62(0·07)	0·74(0·09)	0·24(0·02)	0·23(0·17)
Sum	100	100	97·1(0·8)	97·4(1·2)	96·4(1·4)	96·6(1·2)	98·6(0·3)	98·9(0·5)
An	41·7	36·9	49·2(2·0)	44·3(3·4)	40·8(2·2)	38·1(2·4)	57·3(1·9)	55·3(4·1)
Ab	55·4	57·5	47·0(1·8)	52·2(3·2)	55·3(2·3)	57·2(2·2)	41·3(1·9)	43·4(3·3)
Or	2·9	5·6	3·8(0·6)	3·5(0·4)	3·9(0·5)	4·7(0·6)	1·4(0·2)	1·3(1·1)

T (°C):	900	875	875	875	875	850	850	850
n:	4	3	4	3	3	3	4	2
Charge:	47	81s	86	87s	88s	94	95s	96s
SiO_2	52·5(0·4)	54·5(0·4)	54·6(0·3)	54·6(1·6)	55·4(0·7)	55·8(0·5)	56·6(0·2)	56·1(0·1)
Al_2O_3	29·1(0·4)	27·9(0·1)	27·8(0·1)	28·8(1·0)	27·5(0·3)	26·4(0·6)	26·1(0·1)	26·3(0·1)
FeO*	0·68(0·08)	0·35(0·04)	0·83(0·06)	0·48(0·08)	0·63(0·02)	0·67(0·02)	0·62(0·04)	0·59(0·11)
MgO	0·06(0·02)	0·11(0·02)	0·10(0·01)	0·08(0·04)	0·10(0·02)	0·05(0·01)	0·03(0·01)	0·04(0·01)
CaO	12·89(0·24)	10·88(0·09)	11·52(0·10)	11·87(1·03)	10·93(0·51)	9·53(0·40)	8·67(0·10)	9·42(0·13)
Na_2O	3·98(0·18)	4·92(0·13)	4·53(0·16)	4·48(0·35)	4·78(0·45)	6·00(0·28)	6·07(0·24)	5·85(0·02)
K_2O	0·20(0·04)	0·33(0·01)	0·42(0·05)	0·33(0·11)	0·48(0·06)	0·41(0·06)	0·54(0·04)	0·42(0·03)
Sum	99·4(0·3)	99·1(0·3)	99·9(0·2)	100·6(0·2)	99·8(0·5)	98·8(0·2)	98·7(0·2)	98·8(0·05)
An	63·4(1·5)	54·0(0·9)	57·0(0·8)	58·2(4·3)	54·3(3·2)	45·7(2·2)	42·8(1·3)	46·0(0·3)
Ab	35·4(1·3)	44·1(0·9)	40·5(1·1)	39·8(3·6)	42·8(3·2)	52·0(1·9)	54·1(1·1)	51·6(0·2)
Or	1·2(0·2)	2·0(0·0)	2·5(0·3)	2·0(0·6)	2·8(0·4)	2·3(0·3)	3·2(0·2)	2·4(0·2)

Table 7: Continued

T (°C):	875	875	800	800	825	825	850	850
n:	5	6	7	6	8	8	9	7
Charge:	97	98s	108	109s	133	137s	141cr	142
SiO_2	55·2(1·0)	55·4(1·2)	59·7(1·2)	61·3(0·7)	59·7(0·3)	59·8(0·5)	54·9(2·4)	57·2(1·0)
Al_2O_3	28·6(0·5)	28·4(0·7)	24·9(0·6)	24·2(0·4)	24·5(0·5)	24·9(0·4)	27·8(1·6)	25·5(1·1)
FeO*	0·67(0·10)	0·56(0·1)	0·75(0·20)	0·42(0·07)	0·61(0·08)	0·44(0·08)	0·51(0·17)	0·73(0·07)
MgO	0·06(0·02)	0·08(0·01)	0·07(0·04)	0·05(0·04)	0·05(0·01)	0·05(0·03)	0·04(0·02)	0·21(0·24)
CaO	11·34(0·75)	11·05(0·70)	7·40(0·68)	6·53(0·53)	7·02(0·38)	7·35(0·48)	10·34(1·85)	8·94(0·70)
Na_2O	4·91(0·47)	4·92(0·38)	6·76(0·37)	7·05(0·56)	6·58(0·27)	6·62(0·29)	5·42(1·00)	5·57(0·28)
K_2O	0·35(0·05)	0·35(0·07)	0·58(0·06)	0·54(0·08)	0·61(0·06)	0·52(0·05)	0·29(0·10)	0·50(0·14)
Sum	101·0(0·5)	100·5(0·4)	100·2(0·4)	100·1(0·6)	99·1(0·4)	99·7(0·5)	99·4(0·6)	98·7(0·8)
An	54·9(3·7)	54·3(3·6)	36·4(3·4)	32·8(3·2)	35·7(2·0)	36·9(2·5)	50·5(9·2)	45·6(2·9)
Ab	43·0(3·9)	43·7(3·3)	60·2(3·1)	63·9(3·4)	60·6(1·9)	60·0(2·4)	47·8(8·6)	51·4(2·5)
Or	2·0(0·3)	2·0(0·4)	3·4(0·4)	3·2(0·6)	3·7(0·4)	3·1(0·3)	1·7(0·5)	3·0(0·9)

T (°C):	850	850	850	850	850	875
n:	1	5	7	6	6	1
Charge:	143	144s	146s	148s	184	201
SiO_2	57·9	57·2(1·1)	54·7(0·7)	57·3(0·8)	59·4(1·2)	58·3
Al_2O_3	25·4	26·4(0·7)	27·7(0·7)	25·9(0·3)	24·4(0·7)	25·0
FeO*	0·67	0·26(0·04)	0·43(0·09)	0·59(0·02)	0·55(0·09)	1·4
MgO	0·25	0·11(0·06)	0·06(0·02)	0·15(0·06)	0·05(0·01)	0·25
CaO	8·71	9·20(0·73)	10·28(0·57)	8·87(0·35)	7·19(0·35)	8·35
Na_2O	5·73	5·40(0·40)	5·48(0·33)	5·90(0·22)	6·30(0·36)	6·09
K_2O	0·62	0·41(0·08)	0·25(0·04)	0·44(0·05)	0·77(0·16)	0·65
Sum	99·4	99·4(0·6)	98·9(0·7)	99·2(0·7)	98·7(0·7)	100·2
An	43·9	47·3(3·6)	50·2(2·9)	44·2(1·6)	36·9(1·3)	41·5
Ab	52·3	50·2(3·6)	48·3(2·8)	53·2(1·7)	58·4(1·6)	54·7
Or	3·7	2·5(0·5)	1·5(0·2)	2·6(0·3)	4·7(1·2)	3·9

*Total iron as Fe^{2+}.
An = 100Ca/(Ca + Na + K); Ab = 100Na/(Ca + Na + K); Or = 100K/(Ca + Na + K); n, number of electron microprobe analyses. Numbers in parentheses as in Table 4. Letters after the charge numbers as in Table 6.

under water-saturated conditions. One of Luhr's (1990) experimental results at 200 MPa that could be relevant to the present discussion is that hornblende disappears at $T < 850°C$ only in charges run at high fO_2 and this seems to be related to a significant increase in the clinopyroxene proportion [e.g. charges 153, 149, 105, 144, 165, 139 of Luhr (1990)]. In our experiments with the San Pedro dacite we also found that hornblende disappeared with 1 wt % of added S at high fO_2, and perhaps the disappearance of hornblende in the El Chichón experimental runs was due to the combined effects of the presence of S and high fO_2. The fact that clinopyroxene does not replace hornblende in our S-bearing experiments is probably due to the difference in composition between the El Chichón and San Pedro bulk-rocks and shows that extrapolation of our results on the effect of S in phase equilibria to andesitic compositions is not possible.

Constraints on pre-eruptive conditions

Combining experimental and petrological results, the pre-eruptive conditions of the dacite can be constrained to be 850 ± 10°C, 200 ± 50 MPa, fO_2 of NNO + 1·2 ± 0·1, with about 4·5–5·5 wt % H_2O in the melt, and a bulk S content > 0·1 wt % (and ~300 ppm S in the melt). As shown above (Figs 3, 4 and 6), tight constraints on the temperature and water content can be obtained by comparison of the crystallinity, plagioclase compositions, and mineral proportions between the experimental charges and the natural dacite. The pre-eruptive total

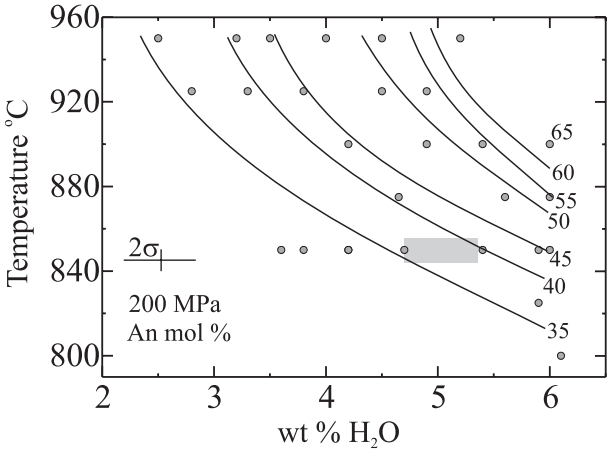

Fig. 6. Variation of the anorthite content (An mol %) of experimental plagioclase with temperature and water content (~200 MPa). Gray box corresponds to the rim composition of the plagioclase phenocrysts of the dacitic lava and the temperature estimated from the Fe–Ti oxides. Only S-free charges have been used to construct the figure.

pressure and its uncertainty is more difficult to assess, but we believe that 200 ± 50 MPa is a good estimate because: (1) experiments at 200 MPa reproduce the range of plagioclase phenocryst compositions found in the lava (An_{65-35}), so that it is not necessary to call upon higher total water pressures to explain the plagioclase compositions; (2) the Al_2O_3 content of hornblende (8·8–9·8 wt %) crystallized at 200 MPa, 850°C, and NNO + 1·4 overlaps with the mean Al_2O_3 content of the hornblende present in the dacite (9·5 ± 0·5 wt % Al_2O_3), whereas the Al_2O_3 content of hornblende crystallized at the same temperature but at 406 MPa (11 ± 1 wt %) is somewhat higher than those of the lava; (3) experimental hornblende is stable only for water contents >4 wt %, which constrains the lowest pre-eruptive pressure to ~100 MPa [using the solubility model of Tamic *et al.* (2001)]; moreover, at 150 MPa, 850°C, and water-saturated conditions, the plagioclase/hornblende values and crystallinity of the charges are already higher than those of the lava, which suggests that the minimum pre-eruptive pressure was >150 MPa. The pre-eruptive fO_2 estimated from the Fe–Ti oxides of the lava (NNO + 1·2) seems also to be in accord with that estimated from experiments. Apart from the changes in phase equilibria as a result of different fO_2, comparison of the *mg*-number of the experimental ferromagnesian minerals and that of the lava can be used to assess the fO_2. The *mg*-number (67 ± 2) of hornblende in the dacite is reproduced at 850°C and at fO_2 of NNO + 1·4 (*mg*-number 67–70), whereas that of orthopyroxene (70 ± 1) lies between the experiments at NNO (61 ± 2) and NNO + 3 (74 ± 2). Finally, the glass composition of the experimental charges at the pre-eruptive conditions noted above overlaps with the glass compositions observed in the dacitic lava (Fig. 5).

As has been noted in the description of the experimental results, the presence of biotite at the pre-eruptive P–T–fO_2–fH_2O conditions that we propose requires the presence of significant amounts of S, at least >0·1 wt %. The glass of charges run at 850°C, NNO + 1·4, and 0·1–1 wt % S contains ~320–360 ppm S, which is very close to the S concentration of the glass inclusions (~300 ppm). The biotite in these same charges has an *mg*-number (70) that is somewhat higher than the range displayed by biotite from the dacitic lava (60–66), which is probably due to a small difference in the redox state. At this fO_2, the experimental charges also contain minor amounts of anhydrite, which is lacking in the dacitic lava. Although one could argue that anhydrite could have been dissolved by rain-water, it could also be that the fO_2 of the dacite was at the lower stability limit for this mineral (e.g. Carroll & Rutherford, 1987; Scaillet & Evans, 1999). It is worth pointing out that if we would have neglected the minor, but very eye-catching, amount of biotite in the lava we could have experimentally reproduced the phase proportions and main mineral assemblage (plagioclase + hornblende ± orthopyroxene) of the dacite without the necessity of adding any S. This highlights the need for detailed and careful petrological and experimental work for fully constraining the pre-eruption conditions and understanding the importance of S in the context of subduction-related volcanism.

In the discussion above we have ignored the presence of clinopyroxene in the dacitic lava, which, as the experiments at 200 MPa show, is not stable at or below 875°C and thus could not have been in equilibrium with the remaining mineral assemblage at the pre-eruptive conditions estimated above. We have considered three possibilities to explain the presence of clinopyroxene in the lava: (1) it could be a xenocryst derived from the QMI; (2) it could have crystallized at lower pressures (e.g. low water contents), as the magma was rapidly ascending to the surface; (3) it could have crystallized at higher temperature (e.g. 900°C) but did not have enough time to re-equilibrate to the lower pre-eruptive temperature, which is our preferred interpretation as we discuss below.

The clinopyroxene composition in the dacite is unlike those found in the quenched mafic inclusions (Costa & Singer, 2002), and thus it seems unlikely that the clinopyroxene is a xenocryst. The fact that experimental charges run at 850°C and low pressure (55 MPa) or low water contents (<3·6 wt % H_2O) do not contain clinopyroxene but orthopyroxene and quartz (which is absent in the dacite) also argues against the possibility that clinopyroxene crystallized at low pressures or water contents as the magma was rising to the surface. Thus, although the phase-equilibrium experiments suggest that the dacitic magma equilibrated most of its mineral assemblage and proportions in a rather restricted range of

Table 8: Experimental magnetite compositions (in wt %)

T (°C):	850	900	900	900	950	950	950	950
n:	1	4	2	3	9	12	6	5
Charge:	1	8	9	10	17	18	19	20
SiO_2	0·00	0·29(0·13)	0·31(0·01)	0·34(0·11)	0·11(0·04)	0·15(0·11)	0·10(0·05)	0·09(0·04)
TiO_2	10·30	2·62(0·04)	3·02(0·03)	3·63(0·06)	7·58(0·37)	7·72(0·26)	8·07(0·15)	8·31(0·14)
Al_2O_3	0·00	3·07(0·09)	2·99(0·06)	2·83(0·08)	1·45(0·06)	1·49(0·07)	1·39(0·03)	1·23(0·02)
FeO*	72·4	82·9(0·4)	82·2(0·4)	82·0(0·8)	77·4(0·9)	77·5(0·8)	77·5(0·4)	77·5(0·3)
MnO	0·45	0·36(0·09)	0·32(0·08)	0·56(0·06)	0·10(0·07)	0·13(0·07)	0·17(0·03)	0·16(0·03)
MgO	1·46	3·06(0·13)	2·98(0·05)	2·93(0·07)	2·28(0·16)	2·29(0·16)	2·23(0·07)	2·08(0·10)
Total[1]	88·8	98·4(0·3)	97·7(0·7)	98·2(0·9)	93·9(0·9)	94·2(0·6)	94·4(0·5)	94·3(0·5)
Fe_2O_3*c*	42·2	60·9(0·3)	59·7(0·3)	59·0(0·6)	49·7(1·0)	49·6(0·6)	49·1(0·3)	48·7(0·2)
FeO*c*	34·4	28·1(0·2)	28·4(0·1)	28·9(0·3)	32·7(0·3)	32·9(0·3)	33·3(0·3)	33·7(0·1)
*X*Ulv	0·31	0·07(0·01)	0·08(0·01)	0·10(0·01)	0·22(0·01)	0·22(0·01)	0·23(0·01)	0·24(0·01)

T (°C):	950	850	850	850	925	875	875	900
n:	2	3	7	4	4	5	5	5
Charge:	21	24	27	28	33	40	41	47
SiO_2	0·63(0·02)	0·31(0·10)	0·31(0·12)	0·47(0·18)	0·37(0·18)	0·42(0·25)	0·25(0·08)	0·34(0·10)
TiO_2	9·26(0·14)	8·77(0·31)	9·18(0·24)	9·56(0·41)	5·97(0·03)	5·96(0·11)	6·92(0·66)	6·33(0·18)
Al_2O_3	1·19(0·01)	1·07(0·04)	0·93(0·05)	0·84(0·05)	1·53(0·04)	3·17(0·10)	2·96(0·09)	3·33(0·07)
FeO*	74·7(0·6)	75·1(0·7)	75·5(0·1)	75·1(0·8)	75·9(0·6)	78·2(0·6)	78·6(0·8)	78·9(0·8)
MnO	0·21(0·01)	0·24(0·02)	0·26(0·02)	0·30(0·02)	1·19(0·12)	0·43(0·05)	0·37(0·05)	0·36(0·02)
MgO	2·14(0·01)	2·58(0·08)	2·54(0·06)	2·34(0·20)	3·09(0·05)	1·81(0·05)	1·84(0·08)	2·01(0·06)
Total[1]	92·8(0·7)	92·8(0·6)	93·4(0·1)	93·3(0·9)	93·7(0·3)	94·9(0·7)	96·0(0·5)	96·4(0·9)
Fe_2O_3*c*	45·9(0·2)	47·2(1·0)	47·1(0·4)	46·2(0·9)	53·1(0·3)	51·3(0·5)	50·4(1·3)	51·5(0·4)
FeO*c*	33·4(0·4)	32·6(0·2)	33·2(0·4)	33·5(0·3)	28·5(0·3)	32·0(0·4)	33·3(0·5)	32·5(0·5)
*X*Ulv	0·27(0·01)	0·25(0·01)	0·26(0·01)	0·27(0·01)	0·16(0·01)	0·19(0·01)	0·21(0·02)	0·19(0·01)

T (°C):	875	875	875	875	850	850	875	800
n:	6	2	7	6	3	5	4	3
Charge:	81s	86	87s	88s	94	95	97	108
SiO_2	0·08(0·03)	0·30(0·01)	0·07(0·03)	0·11(0·07)	0·55(0·05)	0·16(0·01)	0·41(0·22)	0·13(0·02)
TiO_2	5·74(1·61)	6·42(0·02)	5·99(0·80)	6·26(1·08)	6·10(0·03)	6·56(0·08)	10·11(0·08)	13·61(0·86)
Al_2O_3	1·91(0·12)	1·25(0·02)	1·53(0·07)	1·29(0·03)	2·90(0·05)	2·93(0·08)	3·16(0·08)	1·03(0·04)
FeO*	79·3(2·2)	77·4(0·4)	79·4(1·3)	79·3(1·7)	81·4(0·6)	80·0(0·12)	77·5(0·11)	74·8(0·8)
MnO	0·20(0·08)	0·30(0·03)	0·22(0·03)	0·28(0·05)	0·45(0·06)	0·50(0·07)	0·38(0·03)	0·16(0·04)
MgO	2·23(0·79)	2·50(0·02)	2·39(0·41)	2·44(0·47)	1·91(0·08)	1·97(0·10)	1·79(0·05)	1·74(0·11)
Total[1]	94·8(0·5)	93·3(0·4)	95·0(0·6)	95·0(0·3)	98·7(0·6)	97·4(0·2)	97·9(0·3)	95·7(0·2)
Fe_2O_3*c*	53·3(2·7)	51·9(0·3)	53·5(1·4)	53·2(2·1)	54·0(0·3)	52·1(0·2)	45·3(0·3)	39·2(1·9)
FeO*c*	31·4(0·4)	30·7(0·1)	31·3(0·3)	31·4(0·2)	32·8(0·4)	33·1(0·1)	36·7(0·2)	38·6(0·8)
*X*Ulv	0·17(0·04)	0·18(0·01)	0·17(0·02)	0·17(0·03)	0·18(0·01)	0·19(0·01)	0·31(0·01)	0·39(0·02)

T (°C):	800	825	825	850	850	850	850	850
n:	4	5	1	10	3	6	7	5
Charge:	109s	133	137s	141cr	142	143	144s	146s
SiO_2	0·10(0·02)	0·53(0·19)	0·25	0·14(0·03)	0·37(0·22)	0·15(0·06)	0·13(0·04)	0·10(0·03)
TiO_2	13·81(0·89)	6·83(0·07)	6·49	7·84(3·28)	7·11(0·24)	8·19(1·46)	3·97(0·87)	2·60(1·17)
Al_2O_3	1·05(0·05)	2·72(0·07)	2·89	1·00(0·06)	1·06(0·12)	0·84(0·07)	1·33(0·08)	1·77(0·15)
FeO*	73·8(0·7)	78·5(0·8)	76·7	78·3(3·7)	76·5(1·2)	76·9(2·5)	82·0(0·9)	84·4(1·2)
MnO	0·19(0·04)	0·44(0·02)	0·46	0·24(0·10)	0·34(0·01)	0·29(0·10)	0·10(0·07)	0·02(0·01)
MgO	1·65(0·11)	1·57(0·03)	1·90	2·13(0·95)	2·21(0·09)	2·31(0·69)	0·85(0·21)	0·40(0·15)
Total[1]	94·4(0·1)	95·7(0·7)	94·7	94·7(0·4)	92·6(0·6)	93·6(0·8)	94·0(0·7)	95·2(0·2)
Fe_2O_3*c*	38·1(1·6)	50·5(0·5)	50·5	50·2(5·9)	50·1(1·0)	49·0(2·8)	56·1(1·4)	58·8(2·1)
FeO*c*	39·5(0·7)	33·0(0·4)	31·2	33·2(1·8)	31·4(0·3)	32·8(0·5)	31·5(0·8)	31·5(0·8)
*X*Ulv	0·41(0·02)	0·21(0·01)	0·19	0·22(0·09)	0·21(0·01)	0·23(0·04)	0·12(0·03)	0·08(0·04)

T (°C):	850	850	875
n:	5	6	7
Charge:	148s	184	201
SiO_2	0·19(0·03)	0·30(0·14)	0·24(0·11)
TiO_2	7·53(0·61)	8·74(0·11)	6·24(0·39)
Al_2O_3	1·40(0·11)	2·48(0·03)	1·23(0·04)
FeO*	76·4(1·5)	77·5(0·5)	77·3(0·5)
MnO	0·23(0·04)	0·45(0·08)	0·29(0·04)
MgO	2·48(0·35)	1·61(0·06)	2·37(0·14)
Total[1]	93·1(0·8)	95·9(0·9)	92·9(0·13)
Fe_2O_3*c*	49·4(1·5)	47·2(0·3)	51·9(0·7)
FeO*c*	31·9(0·3)	35·0(0·4)	30·6(0·1)
*X*Ulv	0·22(0·02)	0·27(0·01)	0·17(0·01)

*Total iron as Fe^{2+}. *n*, number of electron microprobe analyses. Numbers in parentheses as in Table 4. *X*Ulv, ulvöspinel mole fraction. The letter '*c*' denotes calculated. Letters after the charge numbers as in Table 6.
[1]Total after recalculating the proportions of Fe^{3+} and Fe^{2+} with the structural formula (Stormer, 1983).

P–T–fO_2–fH_2O conditions, the presence of clinopyroxene and the complex zoning of plagioclase phenocrysts indicate that the petrological history of the dacite is more complex than a single near-equilibrium crystallization stage in a shallow magma reservoir. In the following section we integrate the experimental and petrographical results for the dacite with the petrogenetic model proposed by Costa & Singer (2002) for the Holocene zoned eruption of Volcán San Pedro.

Integrating experimental results with magma reservoir dynamics at Volcán San Pedro

Using field, petrographic, and geochemical data, Costa & Singer (2002) proposed a magmatic history for the Holocene San Pedro zoned eruption that can be summarized as follows: (1) the dacite was generated by partial melting of gabbroic rocks; (2) forceful injection of a basaltic magma into the dacite was accompanied by mingling and disaggregation of olivine and plagioclase xenocrysts; (3) the basaltic magma ponded at the base of the dacite and differentiated to basaltic andesite; the dacite was strongly heated at its base and began to convect; (4) differentiated basaltic andesite and a portion of the dacitic reservoir partially mixed to produce the less silicic dacites and andesite; (5) the zoned magma body erupted from its top down.

Detailed information that is particularly illustrative of the dynamics of the San Pedro magma chamber is found in the zoning patterns of plagioclase phenocrysts in the dacite. The main volume of individual crystals consists of normal zoning cycles that oscillate between $An_{65–60}$ and $An_{50–45}$, before they progressively reach compositions of $An_{40–35}$ at the rims (Singer *et al.*, 1995). Such repetitive normal zoning patterns were interpreted by Costa & Singer (2002) as being due to the presence of convection currents caused by a temperature gradient that was induced by the hot mafic magma that ponded at the

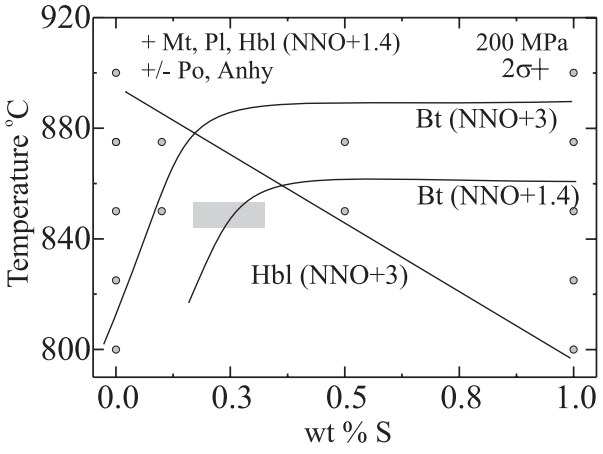

Fig. 7. Phase relations of the San Pedro dacite at ~200 MPa, at various fO_2 values, near H_2O saturation, and with variable amounts of added S (in wt % of the bulk). Noteworthy features are the much larger stability field of biotite and the disappearance of hornblende at high S contents and oxidized conditions, compared with S-free experiments (Fig. 2). Grey box shows the minimum amount of S that is needed to stabilize biotite at the fO_2 and temperature estimated from the Fe–Ti oxides of the dacitic lava. Curves labelled with minerals lying in their stability field. Mineral symbols as in Fig. 2, plus: Po, pyrrhotite; Anhy, anhydrite.

base of the dacite. At 200 MPa, 900°C, and water-saturated conditions the composition of the experimental plagioclase is An_{65}, whereas for the same pressure and water conditions, An_{45} is experimentally reproduced at 850°C, and thus temperature fluctuations could have been ~50°C. It should be noted that between 900 and 850°C both hornblende and plagioclase (the two main minerals of the dacite) are stable, whereas clinopyroxene and An_{65} could have crystallized every time that a portion of the magma reached 900°C. This model assumes that the dacitic magma was open to heat but not mass; notwithstanding, Singer *et al.* (1995) showed that the high-anorthite portions of the plagioclase phenocrysts are correlated with high Fe and Mg peaks, so that it seems plausible that the An_{65} plagioclase crystallized not only in a hotter environment than other parts of the dacite magma, but also from a slightly more mafic composition. Calculated liquids in equilibrium with these high-An zones (Singer *et al.*, 1995) suggest that they crystallized from a magma with ~3–4 wt % MgO, that is 1–2 wt % higher than the dacite bulk-rock. The fact that clinopyroxene is still present in the dacite is probably due to kinetic reasons: it probably did not have enough time to dissolve or re-equilibrate before the magma was erupted. Indeed, the fact that the high-anorthite parts of plagioclase phenocrysts are correlated with high Mg concentrations suggests that the magmatic Mg zoning has not been erased by diffusion (e.g. Costa *et al.*, 2003*a*). Using a simple diffusion equation ($t = x^2/D$, where t is time, x is distance, and D is diffusion coefficient), a distance of 100 μm, 900°C, and a D value from Costa *et al.* (2003*a*) we conclude that the time elapsed between plagioclase crystallization and eruption was less than 100 years.

Is the San Pedro dacite unusual?

With this question we want to address whether the San Pedro dacite should be considered unusual or typical of subduction-related dacites with respect to its pre-eruptive P–T–fO_2–fH_2O conditions and S content. The Mount St. Helens, Katmai, and Pinatubo dacites, for which detailed pre-eruptive conditions have been experimentally determined and which have similar bulk compositions to the San Pedro dacite, contain ≤120 ppm S in glass inclusions (Devine *et al.*, 1984; Palais & Sigurdsson, 1989; Westrich *et al.*, 1991; Westrich & Gerlach, 1992), which is significantly lower than the ~300 ppm S that we have inferred for the San Pedro dacite from experimental and glass-inclusion data. Such a difference could be attributed to: (1) differences in the pre-eruptive intensive parameters or glass compositions; (2) differences in the primary S contents. The low S contents inferred for the Katmai dacite could readily be explained as being due to the low volatile solubility at the estimated pre-eruptive pressure of 25–50 MPa (Hammer *et al.*, 2002). In contrast, the main pre-eruptive stage of the Mount St. Helens dacite has been determined to be 220 MPa, 930°C, NNO + 1·2 (Rutherford *et al.*, 1985; Gardner *et al.*, 1995), and we could expect an amount of S similar to the San Pedro dacite. Thus, the low S content of glass inclusions from Mount St. Helens dacite (~68 ppm; Devine *et al.*, 1984) is probably due to the low S content of the magma, unless glass inclusions were formed during the protracted polybaric crystallization of the dacitic magma towards much lower pressures (down to 11 MPa; Blundy & Cashman, 2001). This is not the case for the Pinatubo dacite, for its pre-eruptive pressure has been estimated at 220 MPa (Rutherford & Devine, 1996; Scaillet & Evans, 1999). None the less, the much lower estimated pre-eruptive temperature (760°C) and the high silica content of the glass (77 wt % SiO_2) probably determined its much lower S content, because S solubility decreases with falling temperature and increasing silica (Clemente *et al.*, in preparation). Apart from these three examples, there are other subduction-related dacites in which S contents similar to those of the San Pedro dacite have been reported. The glass inclusions in phenocrysts of the 1902 dacite from Volcán Santa María in Guatemala contain ~200 ppm S (Rose, 1987; Palais & Sigurdsson, 1989), those from the 1989 eruption of Volcán Lascar in Chile contain ~50–400 ppm S (at 72–75 wt % SiO_2; Matthews *et al.*, 1999), those from the 1400 BP eruption of Rabaul contain 314–614 ppm S (Palais & Sigurdsson, 1989), and those from the AD 1600 Huaynaputina eruption contain ~265 ppm S (Costa *et al.*, 2003*b*). Thus the relatively high S content and its effect on the phase

equilibria that we report for the San Pedro dacite is probably due to a combination of P–T–fO_2, and probably also to high magmatic S contents. The S in the San Pedro dacite could be a feature inherited from the source or acquired in the magmatic reservoir for which we have inferred the pre-eruptive conditions. Using petrological and geochemical data, Costa & Singer (2002) proposed that the San Pedro dacite was likely to be the result of partial melting of gabbroic rocks, similar to the gabbroic xenoliths found in the lavas of the eruption. If this scenario is correct then the high S content of the dacite could well be a source feature, as the gabbroic xenoliths contain abundant pyrrhotite and in some cases apatite with high S contents (Costa, 2000). On the other hand, the fact that there was a mafic magma coexisting with the dacite in the magma reservoir opens the possibility that volatiles, including sulphur, were transferred from the mafic magma to the dacite (e.g. Andres *et al.*, 1991).

CONCLUSIONS

This study shows that S should be considered in petrological and experimental studies of arc magmas for a comprehensive understanding of their mineral assemblages and pre-eruptive conditions. Moreover, to reconcile petrographic data and experimental results for the San Pedro dacite it was necessary to: (1) perform S-free and S-bearing experiments to constrain the pre-eruptive conditions (200 ± 50 MPa, 850 ± 10°C, 4·5–5·5 wt % H_2O in the melt, and >0·1 wt % S bulk and ~300 ppm S in the melt, at NNO + 1·2 ± 0·2); S-bearing experiments show that the phase equilibria of oxidized (>NNO + 1·2) dacitic magmas will be significantly affected by the presence of 0·5–1 wt % S bulk or high S concentrations in the melt (e.g. >300 ppm); (2) take into account the zoning patterns of plagioclase phenocrysts and the Holocene San Pedro magmatic history to explain the presence of high-temperature minerals (e.g. clinopyroxene) and mineral compositions (high anorthite content in plagioclase) in the dacitic lava by short-lived (<100 years) temperature fluctuations (e.g. 50°C) in the magma reservoir.

ACKNOWLEDGEMENTS

We would like to thank R. Champallier for his assistance during the experiments, B. Singer for providing mineral separates of the dacite, and F. Parat, M. Dungan, and S. Chakraborty for discussions that improved the manuscript. The assistance of O. Rouer and H.-J. Bernhardt during microprobe analyses is gratefully acknowledged. Constructive reviews by J. Luhr, J. Hammer, and particularly M. Carroll are greatly appreciated and helped to improve the text and clarify the discussion in several ways. F.C. acknowledges the generous financial support of the EC by a Marie Curie Fellowship of the program Improving Human Research Potential and the Socio-economic Knowledge Base under contract number HPMFCT-2000-00493.

REFERENCES

Albarède, F. (1995). *Introduction to Geochemical Modeling*. Cambridge: Cambridge University Press, 543 pp.

Andersen, D. J. & Lindsley, D. H. (1988). Internally consistent solution models for Fe–Mg–Mn–Ti oxides: Fe–Ti oxides. *American Mineralogist* **73**, 714–726.

Andersen, D. J., Lindsley, D. H. & Davidson, P. M. (1993). QUILF: a Pascal program to assess equilibria among Fe–Mg–Ti oxides, pyroxenes, olivine and quartz. *Computers and Geosciences* **19**, 1333–1350.

Andres, R. J., Rose, W. I., Kyle, P. R., De Silva, S., Francis, P., Gardeweg, M. & Moreno Roa, H. (1991). Excessive sulfur dioxide emissions from Chilean volcanoes. *Journal of Volcanology and Geothermal Research* **46**, 323–329.

Bacon, C. R. & Hirschmann, M. M. (1988). Mg/Mn partitioning as a test for equilibrium between coexisting oxides. *American Mineralogist* **73**, 57–61.

Barclay, J., Rutherford, M. J., Carroll, M. R., Murphy, M. D., Devine, J. D., Gardner, J. & Sparks, R. S. J. (1998). Experimental phase equilibria constraints on pre-eruptive storage conditions of the Soufriere Hills magma. *Geophysical Research Letters* **25**, 3437–3440.

Blundy, J. D. & Cashman, K. (2001). Ascent-driven crystallisation of dacite magmas at Mount St. Helens, 1980–1986. *Contributions to Mineralogy and Petrology* **140**, 631–650.

Burnham, C. W., Holloway, J. R. & Davis, N. F. (1969). Thermodynamic properties of water to 1000°C and 10000 bar. *Geological Society of America, Special Papers* **132**, 1–96.

Carroll, M. C. & Rutherford, M. J. (1985). Sulfide and sulfate saturation in hydrous silicate melts. *Journal of Geophysical Research* **90**(Supplement), C601–C612.

Carroll, M. C. & Rutherford, M. J. (1987). The stability of igneous anhydrite: experimental results and implications for sulfur behavior in the 1982 El Chichón trachyandesite and other evolved magmas. *Journal of Petrology* **28**, 781–801.

Carroll, M. C. & Webster, J. D. (1994). Solubilities of sulfur, noble gases, nitrogen, chlorine, and fluorine in magmas. In: Carroll, M. R. & Holloway, J. R. (eds) *Volatiles in Magmas. Mineralogical Society of America, Reviews in Mineralogy* **30**, 231–279.

Costa, F. (2000). The petrology and geochemistry of diverse crustal xenoliths, Tatara–San Pedro volcanic complex, Chilean Andes. Ph.D. thesis, University of Geneva, 120 pp.

Costa, F. & Singer, B. S. (2002). Evolution of Holocene dacite and compositionally zoned magma, Volcán San Pedro, Southern Volcanic Zone, Chile. *Journal of Petrology* **43**, 1571–1593.

Costa, F., Dungan, M. & Singer, B. S. (2002). Hornblende- and phlogopite-bearing gabbroic xenoliths from Volcán San Pedro (36°S), Chilean Andes: evidence for melt and fluid migration and reactions in subduction-related plutons. *Journal of Petrology* **43**, 219–241.

Costa, F., Chakraborty, S. & Dohmen, R. (2003*a*). Diffusion coupling between trace and major elements and a model for calculation of magma residence times using plagioclase. *Geochimica et Cosmochimica Acta* **67**, 2189–2200.

Costa, F., Scaillet, B. & Gourgaud, A. (2003*b*). Massive atmospheric sulfur loading of the AD 1600 Huaynaputina eruption and implications for petrologic sulfur estimates. *Geophysical Research Letters* **30**, 1068, doi: 10.1029/2002GL016402.

Cottrell, E., Gardner, J. E. & Rutherford, M. J. (1999). Petrologic and experimental evidence for the movement and heating of the pre-

eruptive Minoan rhyodacite (Santorini, Greece). *Contributions to Mineralogy and Petrology* **135**, 315–331.

Deer, W. A., Howie, R. A. & Zussman, J. (1992). *An Introduction to the Rock-forming Minerals*. Harlow: Longman, 696 pp.

Devine, J. D., Sigurdsson, H., Davis, A. N. & Self, S. (1984). Estimates of sulfur and chlorine yield to the atmosphere from volcanic eruptions and potential climatic effects. *Journal of Geophysical Research* **89**, 6309–6325.

Dungan, M., Wulff, A. & Thompson, R. (2001). A refined eruptive stratigraphy for the Tatara–San Pedro Complex (36°S, Southern Volcanic Zone, Chilean Andes): reconstruction methodology and implications for magma evolution at long-lived arc volcanic centers. *Journal of Petrology* **42**, 555–626.

Feeley, T. C. & Dungan, M. A. (1996). Compositional and dynamic controls on mafic–silicic magma interactions at continental arc volcanoes: evidence from Cordón El Guadal, Tatara–San Pedro Complex, Chile. *Journal of Petrology* **37**, 1547–1577.

Ferguson, K. M., Dungan, M., Davidson, J. P. & Colucci, M. T. (1992). The Tatara–San Pedro volcano, 36°S Chile: a chemically variable, dominantly mafic magmatic system. *Journal of Petrology* **33**, 1–43.

Fougnot, J., Pichavant, M. & Barbey, P. (1996). Biotite resorption in dacite lavas from northeastern Algeria. *European Journal of Mineralogy* **8**, 625–638.

Gardner, J. E., Rutherford, M., Carey, S. & Sigurdsson, H. (1995). Experimental constraints on pre-eruptive water contents and changing magma storage prior to explosive eruptions of Mount St. Helens volcano. *Bulletin of Volcanology* **57**, 1–17.

Gerlach, T. M., Westrich, H. R. & Symonds, R. B. (1996). Pre-eruption vapor in magma of the climactic Mount Pinatubo eruption: source of the giant stratospheric sulfur dioxide cloud. In: Newhall, C. G. & Punongbayan, R. S. (eds) *Fire and Mud. Eruptions of Lahars of Mount Pinatubo, Philippines*. Seattle: University of Washington Press, pp. 415–434.

Ghiorso, M. & Sack, R. (1991). Fe–Ti oxides geothermometry: thermodynamic formulation and the estimation of intensive variables in silicic magmas. *Contributions to Mineralogy and Petrology* **108**, 485–510.

Hammer, J. E., Rutherford, M. J. & Hildreth, W. (2002). Magma storage prior to the 1912 eruption at Novarupta, Alaska. *Contributions to Mineralogy and Petrology* **144**, 144–162.

Hildreth, W. & Drake, R. E. (1992). Volcán Quizapu, Chilean Andes. *Bulletin of Volcanology* **54**, 93–125.

Hildreth, W. & Moorbath, S. (1988). Crustal contributions to arc magmatism in the Andes of Central Chile. *Contributions to Mineralogy and Petrology* **98**, 455–489.

Huebner, J. S. & Sato, M. (1970). The oxygen fugacity–temperature relationships of manganese nickel oxide buffers. *American Mineralogist* **55**, 934–956.

Johnson, M. C., Anderson, A. T. & Rutherford, M. C. (1994). Pre-eruptive volatile contents of magmas. In: Carroll, M. R. & Holloway, J. R. (eds) *Volatiles in Magmas. Mineralogical Society of America, Reviews in Mineralogy* **30**, 281–330.

Leake, B. E., Woolley, A. R., Arps, C. E. S., Birch, W. D., Gilbert, M. C., Grice, J. D., *et al.* (1997). Nomenclature of amphiboles: report of the Subcommittee on Amphiboles of the International Mineralogical Association, commission on new minerals and minerals names. *American Mineralogist* **82**, 1019–1037.

Luhr, J. (1990). Experimental phase relations of water and sulfur-saturated arc magmas and the 1982 eruptions of El Chichón volcano. *Journal of Petrology* **31**, 1071–1114.

Manley, C. & Bacon, C. R. (2000). Rhyolite thermobarometry and the shallowing of the magma reservoir, Coso volcanic field, California. *Journal of Petrology* **41**, 149–174.

Martel, C., Pichavant, M., Bourdier, J.-L., Traineau, H., Holtz, F. & Scaillet, B. (1998). Magma storage conditions and control of eruption regime in silicic volcanoes: experimental evidence from Mt. Pelée. *Earth and Planetary Science Letters* **156**, 89–99.

Martel, C., Pichavant, M., Holtz, F., Scaillet, B., Bourdier, J.-L. & Traineau, H. (1999). Effects of fO_2 and H_2O on andesite phase relations between 2 and 4 kbar. *Journal of Geophysical Research* **104**, 29453–29470.

Matthews, S. J., Sparks, R. S. J. & Gardeweg, M. C. (1999). The Piedras Grandes–Soncor eruptions, Lascar volcano, Chile; evolution of a zoned magma chamber in the Central Andean upper crust. *Journal of Petrology* **40**, 1891–1919.

Palais, J. M. & Sigurdsson, H. (1989). Petrologic evidence of volatile emissions from major historic and pre-historic volcanic eruptions. In: Berger, A. L., Dickinson, R. E. & Kidson, J. (eds) *Understanding Climate Change. Geophysical Monograph, American Geophysical Union* **52**, 31–53.

Pichavant, M., Martel, C., Bourdier, J.-L. & Scaillet, B. (2002). Physical conditions, structure and dynamics of a zoned magma chamber: Mt. Pelée (Martinique, Lesser Antilles Arc). *Journal of Geophysical Research* **107**, doi: 10.1029/2001JB000315.

Popp, R. K., Gilbert, M. C. & Craig, J. R. (1977). Stability of Fe–Mg amphiboles with respect to sulfur fugacity. *American Mineralogist* **62**, 13–30.

Pownceby, M. I. & O'Neill, H. St. C. (1994). Thermodynamic data from redox reactions at high temperatures. III. Activity–composition relations in Ni–Pd alloys from EMF measurements at 850–1250 K, and calibration of the NiO + Ni–Pd assemblage as a redox sensor. *Contributions to Mineralogy and Petrology* **116**, 327–339.

Robie, R. A., Hemingway, B. S. & Fisher, J. R. (1979). Thermodynamic properties of minerals and related substances at 298·15 K and 1 bar (10^5 pascals) pressure and at higher temperature. *US Geological Survey Bulletin* **1452**.

Robock, A. (2000). Volcanic eruptions and climate. *Reviews of Geophysics* **38**, 191–219.

Rose, W. I. (1987). Santa María, Guatemala: bimodal, soda-rich calc-alkalic stratovolcano. *Journal of Volcanology and Geothermal Research* **33**, 109–129.

Roux, J. & Lefèvre, A. (1992). A fast quench device for internally heated pressure vessels. *European Journal of Mineralogy* **4**, 279–281.

Rutherford, M. J. & Devine, J. D. (1996). Pre-eruption pressure–temperature conditions and volatiles in the 1991 Mount Pinatubo magma. In: Newhall, C. G. & Punongbayan, R. S. (eds) *Fire and Mud, Eruptions and Lahars of Mount Pinatubo, Philippines*. Seattle: University of Washington Press, pp. 751–766.

Rutherford, M. J. & Hill, P. M. (1993). Magma ascent rates from amphibole breakdown: an experimental study applied to the 1980–1986 Mount St. Helens eruptions. *Journal of Geophysical Research* **98**, 19667–19685.

Rutherford, M. J., Sigurdsson, H. & Carey, S. (1985). The May 18, 1980, eruption of Mount St. Helens, 1. Melt compositions and experimental phase equilibria. *Journal of Geophysical Research* **90**, 2929–2947.

Sato, H., Nakada, S., Fujii, T., Nakamura, M. & Suzuki-Kamata, K. (1999). Groundmass pargasite in the 1991–1995 dacite of Unzen volcano: phase stability experiments and volcanological implications. *Journal of Volcanology and Geothermal Research* **89**, 197–212.

Scaillet, B. & Evans, W. E. (1999). The 15 June 1991 eruption of Mount Pinatubo. I. Phase equilibria and pre-eruption P–T–fO_2–fH_2O conditions of the dacite magma. *Journal of Petrology* **40**, 381–411.

Scaillet, B. & Pichavant, M. (2003). Experimental constraints on volatile abundances in arc magmas and their implications for degassing processes. In: Oppenheimer, C., Pyle, D. & Barclay, J. (eds) *Volcanic Degassing. Geological Society, London, Special Publications* **213**, 23–52.

Scaillet, B., Pichavant, M., Roux, J., Humbert, G. & Lefèvre, A (1992). Improvements of the Shaw membrane technique for measurement and control of $f\,H_2$ at high temperatures and pressures. *American Mineralogist* **77**, 647–655.

Scaillet, B., Pichavant, M. & Roux, J. (1995). Experimental crystallization of leucogranite magmas. *Journal of Petrology* **36**, 663–705.

Schmidt, B. C., Scaillet, B. & Holtz, F. (1995). Accurate control of $f\,H_2$ in cold seal pressure vessels with the Shaw membrane technique. *European Journal of Mineralogy* **7**, 893–903.

Singer, B. S., Dungan, M. A. & Layne, G. D. (1995). Textures and Sr, Ba, Mg, Fe, K, and Ti compositional profiles in volcanic plagioclase: clues to the dynamics of calc-alkaline magma chambers. *American Mineralogist* **80**, 776–798.

Singer, B. S., Thompson, R. A., Dungan, M. A., Feeley, T. C., Nelson, S. T., Pickens, J. C., Brown, L. L., Wulff, A. W., Davidson, J. P. & Metzger, J. (1997). Volcanism and erosion during the past 930 k.y. at the Tatara–San Pedro complex, Chilean Andes. *Geological Society of America Bulletin* **109**, 127–142.

Stormer, J. C. (1983). The effects of recalculation on estimates of temperature and oxygen fugacity from analyses of multi-component iron–titanium oxides. *American Mineralogist* **68**, 586–594.

Tamic, N., Behrens, H. & Holtz, F. (2001). The solubility of H_2O and CO_2 in rhyolitic melts in equilibrium with a H_2O–CO_2 mixed fluid phase. *Chemical Geology* **174**, 333–347.

Tso, J. L., Gilbert, M. L. & Craig, J. R. (1979). Sulfidation of synthetic biotites. *American Mineralogist* **64**, 304–316.

Westrich, H., Eichelberger, J. C. & Hervig, R. L. (1991). Degassing of the 1912 Katmai magmas. *Geophysical Research Letters* **8**, 1561–1564.

Westrich, H. R. & Gerlach, T. M. (1992). Magmatic gas source for the stratospheric SO_2 cloud from the June, 1991, eruption of Mount Pinatubo. *Geology* **20**, 867–870.